Higher MLCT Lifetime of Carbene Iron(II) Complexes by Chelate Ring Expansion

Thomas Reuter, Ayla Kruse, Roland Schoch, Stefan Lochbrunner, Matthias Bauer and Katja Heinze

Supplementary Information

General

All reactions and measurements were performed under argon atmosphere unless otherwise noted. An analytic- and a synthesis glovebox (UniLab/MBraun – Ar 4.8, O_2 < 1 ppm, H_2O < 0.1 ppm) were used to store and weigh sensitive compounds for synthesis as well as to prepare any measurement sample that required absence of oxygen and water. Dichloromethane, acetonitrile and CD_3CN were dried and distilled from calcium hydride and stored over molecular sieve (3 Å). THF was dried from potassium and distilled prior to use. The reagents were used as received from commercial suppliers (ABCR, Acros Organics, Alfa Aesar, Fischer Scientific, Fluka and Sigma-Aldrich). Deuterated solvents were purchased from euriso-top and Deutero GmbH.

^{1}H and ^{13}C{^{1}H} NMR spectra were recorded on a *Bruker Avance DRX 400* spectrometer at 400.31 MHz(^{1}H), 100.05 MHz (^{13}C{^{1}H}). Chemical shifts (δ) are reported to the shift scale calibrated with the residual non-deuterated NMR solvent; CH_2Cl_2 (5.32 ppm for ^{1}H NMR) and CD_3CN (1.94 ppm for ^{1}H NMR and 1.32 and 118.26 ppm for ^{13}C{^{1}H} NMR).[1]

Electrospray ionization mass spectra were recorded on an *Agilent 6545 QTOF-MS* spectrometer.

The **elemental analysis** was performed by the microanalytical laboratory of the department of chemistry of the University of Mainz on a *vario EL cube* from *Elementar*.

IR spectra were recorded on a *Bruker Alpha II* FTIR spectrometer with an ATR unit containing a diamond crystal.

UV/Vis/NIR spectra were recorded on a *Varian Cary 5000* spectrometer and a *Jasco V-770* spectrometer using 1.0 cm cells (Hellma, Suprasil).

Electrochemical experiments of **[Fe(dpmi)$_2$][PF$_6$]$_2$** were carried out on a *BioLogic SP-200* voltammetric analyzer using a platinum working electrode, a platinum wire as counter electrode and a 0.01 M Ag/AgNO$_3$ in CH_3CN reference electrode. The measurements were carried out at a scan rate of 100 mV s^{-1} for cyclic voltammetry experiments using 0.1 M [^{n}Bu$_4$][PF$_6$] as supporting electrolyte and 0.001 M of the sample in acetonitrile. Potentials are referenced relative to the ferrocene/ferrocenium couple.

Spectroelectrochemical measurements of **[Fe(dpmi)$_2$][PF$_6$]$_2$** were performed on a *BioLogic SP-50* voltammetric analyser using a *Specac omni-cell* liquid transmission cell[2] with CaF$_2$ windows equipped with a Pt gauze working electrode and an Ag wire as pseudo-reference electrode, melt-sealed in a self-made polyethylene spacer (approximate 0.5 mm path length) containing 0.1 M [^{n}Bu$_4$][PF$_6$] in acetonitrile.

X-ray absorption spectroscopic measurements of **[Fe(dpmi)$_2$][PF$_6$]$_2$** were carried out at PETRA III beamline P65 at Deutsches Elektronensynchrotron (DESY) in Hamburg, Germany. The measurements at the iron K-edge (7112 eV) were performed using a Si(111) double-crystal monochromator in continuous scans (180 s per scan) and a maximum synchrotron beam current of 100 mA. Spectra were

recorded in transmission mode in solid form as pellets diluted in boron nitride. The preparation of the sample was carried out under inert atmosphere in a glove box. For energy calibration, an iron foil was measured simultaneously with the sample.

EXAFS data analysis

In the first step of data analysis, the background of the spectrum was removed by subtracting a Victoreen-type polynomial.[3] E_0 was defined as the first inflection point in the edge – which was determined using the first maximum in the first derivative. Afterwards a piecewise polynomial was used to determine the smooth part of the spectrum and was adjusted in a way that the low-R components of the resulting Fourier transform were minimal. The background-subtracted spectrum was divided by its smoothed part and the photon energy was converted to photoelectron wave number k. For evaluation of the EXAFS spectra the resulting functions were weighted with k^3 and calculated with EXCURVE98, which works based on the EXAFS function and according to a formulation in terms of radial distribution functions.[4,5]

$$\chi(k) = \sum_j S_0^2(k) F_j(k) \int P_j(r_j) \frac{e^{\frac{-2r_j}{\lambda}}}{k r_j^2} \sin\left[2k r_j + \delta_j(k)\right] dr_j$$

The number of independent points N_{ind} was calculated according to information theory to determine the degree of overdeterminacy.[5]

$$N_{ind} = \frac{2\Delta k \Delta R}{\pi}$$

Here, Δk describes the range in k-space used for data analysis and ΔR corresponds to the distance range in the Fourier filtering process. For the analysis a Δk-range of 9 and a ΔR-range of 5 was used, which yielded a number of independent points of 28. The quality of a fit was determined using two methods. The reduced χ_{red}^2 considers the degree of overdeterminacy of the system and the number of fitted parameters p. It therefore allows a direct comparison of different models:[6]

$$\chi_{red}^2 = \frac{\binom{N_{ind}}{N}}{N_{ind} - p} \sum_i \left(\frac{k_i^n}{\sum_j k_j^n \left| \chi_j^{exp}(k_j) \right|} \right)^2 (\chi^{exp}(k_i) - \chi^{theo}(k_i))^2$$

The R-factor, which represents the percental disagreement between experiment and adjusted function and takes into account both systematic and random errors according to the equation:[6]

$$R = \sum_i \frac{k_i^n}{\sum_j k_j^n \left| \chi_j^{exp}(k_j) \right|} \left| \chi^{exp}(k_i) - \chi^{theo}(k_i) \right| \cdot 100\%$$

The accuracy of the determined distances is 1 %, of the Debye-Waller-like factor 10 %[7] and of the coordination numbers depending of the distance 5 – 15 %. Initial values for coordination numbers and distances were adopted from Rietveld-analysis and afterwards iterated free in every fit as well as the Debye-Waller-like factor and the amplitude reducing factor.

Transient absorption spectra of **[Fe(dpmi)₂][PF₆]₂** were recorded applying a pump-probe setup with an excitation wavelength set to 490 nm.[8] The setup is pumped by a Ti:Sapphire laser system (Spectra-Physics, Spitfire Pro) which provides ultrashort laser pulses centred at 775 nm with a repetition rate of 1 kHz. A non-collinear optical parametric amplifier (NOPA) tuned to a centre wavelength of 490 nm delivered the excitation pulses whose dispersion was controlled by prism compressor. For probing, a white light continuum generated with a CaF₂ crystal was used. Both beams, with polarizations arranged

in magic angle, were focused onto the sample leading to pump and probe spots with diameters of 390 μm and 120 μm, respectively. Transient absorption spectra were recorded by dispersing the probe beam after the sample with a prism and detecting its spectral intensity distribution with a CCD array. The metal complex was dissolved in acetonitrile under argon atmosphere and the obtained sample was filled into a 1 mm fused silica cuvette. The concentration was 2.8×10^{-4} M resulting in an optical density of 0.43 at 490 nm.

Density functional theory calculations of **1²⁺** were executed with Orca 4.1.1[9,10] using the Elwetritsch or MOGON high performance computing facilities. The B3LYP[11-13] formulation of DFT and Def2-tzvp[14,15] as basis set which uses polarization functions for non-hydrogen atoms were employed. For solvent modelling, CPCM[16,17] in CH_3CN was applied. The "zeroth order regular approximation" (ZORA)[14] was used for relativistic corrections. The RIJCOSX[18,19] approximation was used along with the auxiliary basis set Def2/J[14,15] to accelerate the calculations. Atom-pairwise dispersion correction was performed with the Becke-Johnson damping scheme (D3BJ).[20,21] The character of the states was assigned by dividing the molecule into fragments and calculating charge transfer numbers, as implemented in the TheoDore software package.[22-24] For an initial charge transfer number analysis, the complex was divided into three fragments (iron centre and the two tripodal ligands), while for a more detailed analysis the ligands were further partitioned into two parts themselves (pyridine and carbene fragment).

Synthesis
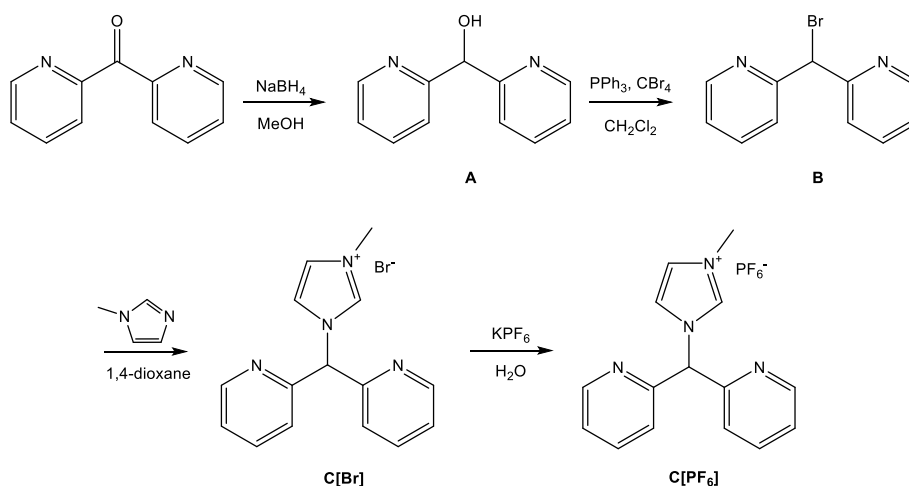
Di(pyridine-2-yl)methanol (A): 1 g (5.43 mmol, 1 eq.) di(pyridine-2-yl)methanone were stirred in methanol (20 mL) at 0 °C. 205.37 mg (5.43 mmol, 1 eq.) NaBH$_4$ were slowly added. The resulting solution was stirred for 1 h at 0 °C and 12 h at room temperature. The solvent was evaporated under reduced pressure and the resulting residue dissolved in 2 M hydrochloric acid and stirred for 10 min. The pH of the solution was adjusted to 8 using NH$_4$OH$_{(aq)}$. The aqueous solution was extracted with dichloromethane. After drying the organic phase with MgSO$_4$, the solvent was removed under reduced pressure giving the product as a pale brown oil (991 mg, 5.32 mmol, 98 %). ^{1}H NMR (400 MHz, CD$_2$Cl$_2$): $\delta = 8.53$ (d, 2H), 7.66 (td, 2H), 7.51 (d, 2H), 7.20 (m, 2H), 5.84 (d, 1H), 5.72 (d, 1H) ppm.

2,2'-(Bromomethylene)dipyridine (B): 2.01 g (10.8 mmol, 1 eq.) di(pyridine-2-yl)methanol and 7.16 g (21.59 mmol, 1.99 eq.) CBr$_4$ were dissolved in dichloromethane (20 mL) and cooled to 0 °C. 3.94 g (11.88 mmol, 1.1 eq.) of PPh$_3$ were added in small portions. The mixture was stirred for 1.5 h. After removal of the solvent under reduced pressure, the residue was purified by column chromatography on silica with ethyl acetate as eluent, giving the product as a colourless solid (1.75 g, 7.03 mmol, 65 %). ^{1}H NMR (400 MHz, CD$_3$CN): $\delta = 8.52$ (d, 2H), 7.81 − 7.74 (m, 4H), 7.27 (t, 2H), 6.33 (s, 1H) ppm.

1-(Di(pyridin-2-yl)methyl)-3-methyl-1H-imidazol-3-ium hexafluorophosphate (C[PF$_6$]) (analogous to ref. 25): 528.83 mg (2.12 mmol, 1 eq.) 2,2'-(bromomethylene)dipyridine and 0.37 mL (4.67 mmol, 2.2 eq.) methylimidazole were refluxed in 1,4-dioxane (30 mL) for 48 h. The resulting precipitate was collected and dried under reduced pressure giving 561.75 mg (1.70 mmol, 80 %) 1-(di(pyridin-2-yl)methyl)-3-methyl-1H-imidazol-3-ium bromide. The hexafluorophosphate salt of the pro-ligand was obtained by dissolving the bromide salt in water (20 mL) and adding an aqueous solution of KPF$_6$ (3 eq.) whereby 1-(di(pyridin-2-yl)methyl)-3-methyl-1H-imidazol-3-ium hexafluorophosphate precipitated (639.99 mg, 1.62 mmol, 95 %). ^{1}H NMR (400 MHz, CD$_3$CN): $\delta = 8.88$ (s, 1H), 8.58 (d, 2H), 7.84 (td, 2H), 7.61 (t, 1H), 7.43 − 7.37 (m, 5H), 6.95 (2, 1H), 3.86 (s, 3H) ppm.

[Fe(dpmi)$_2$][PF$_6$]$_2$: 396.28 mg (1 mmol, 2 eq.) 1-(di(pyridin-2-yl)methyl)-3-methyl-1H-imidazol-3-ium hexafluorophosphate were suspended in dry THF (25 mL) and cooled to −70 °C in an ethanol/dry ice bath. Addition of a solution of 112.21 mg (1 mmol, 2 eq.) KO^{t}Bu in dry THF (10 mL) yielded a clear orange solution. After 10 min stirring at −70 °C, a solution of 107.83 mg (0.5 mmol, 1 eq.) FeBr$_2$ in dry THF (20 mL) was added. The resulting mixture was slowly warmed to room temperature and left stirring overnight. An orange precipitate formed. The solvent was removed under reduced pressure. The residue was dissolved in acetonitrile (5 mL), filtered and the product precipitated with diethyl ether giving **[Fe(dpmi)$_2$][PF$_6$]$_2$** as an orange powder (352.1 mg, 0.42 mmol, 83 %). ^{1}H NMR (400 MHz, CD$_3$CN): $\delta = 8.12$ (d, 2H), 8.03 (t, 2H), 7.90 (m, 4H), 7.80 (t, 2H), 7.38 (m, 4H), 7.25 (d, 2H), 7.21 (d, 2H), 7.15 (t,

2H), 6.87 (t, 2H), 2.44 (s, 6H) ppm. $^{13}C\{^1H\}$ NMR (400 MHz, CD_3CN): 199.12, 160.71, 159.69, 159.05, 157.92, 139.27, 138.56, 126.36, 126.15, 125.31, 125.14, 125.06, 123.58, 66.36, 35.50 ppm. IR (ATR): $\tilde{\upsilon}$ = 1607 (w), 1566 (w), 1475 (m), 1445 (m), 1420 (m), 1401 (m), 1354 (w), 1332 (w), 1313 (w), 1266 (w), 1244 (w), 1214 (w), 1196 (m), 1170 (w), 1075 (w), 877 (m), 835 (s, PF_6), 771 (m), 756 (m), 738 (m), 723 (m), 694 (m), 657 (m), 557 (s, PF_6), 522 (m), 492 (w), 467 (w), 423 (m) cm^{-1}. ESI$^+$-MS (m/z): 278.09 [**1**]$^{2+}$, 701.14. [**1^{2+}**+PF_6^-]$^+$. UV/Vis (CH_3CN): λ (ε/ L mol^{-1} cm^{-1}) = 255 (39700), 415 nm (17310), 500 nm (19390). Elemental analysis for $C_{30}H_{28}F_{12}FeN_8P_2$: calcd. C 42.57 %, H 3.33 %, N 13.24 %; found C 42.57 %, H 3.19 %, N 12.96 %.

Oxidation to iron(III). The iron(III) complex was obtained in situ by dissolving **[Fe(dpmi)$_2$][PF$_6$]$_2$** (15 mg, 17.72 mmol) in CH_3CN (5 mL) or ^{n}PrCN (5 mL) and adding [NO][PF$_6$] (3.1 mg, 17.72 mmol) as a solid. The colour of the solution changed from orange to blue. Gas evolution was not observed. This solution was appropriately diluted with the respective solvent and used for absorption and emission experiments. Low temperature emission spectroscopy (77 K) was performed in ^{n}PrCN. UV/Vis (CH_3CN): λ (ε/ L mol^{-1} cm^{-1}) = 338 (5500), 525 nm (3080), 609 nm (3460).
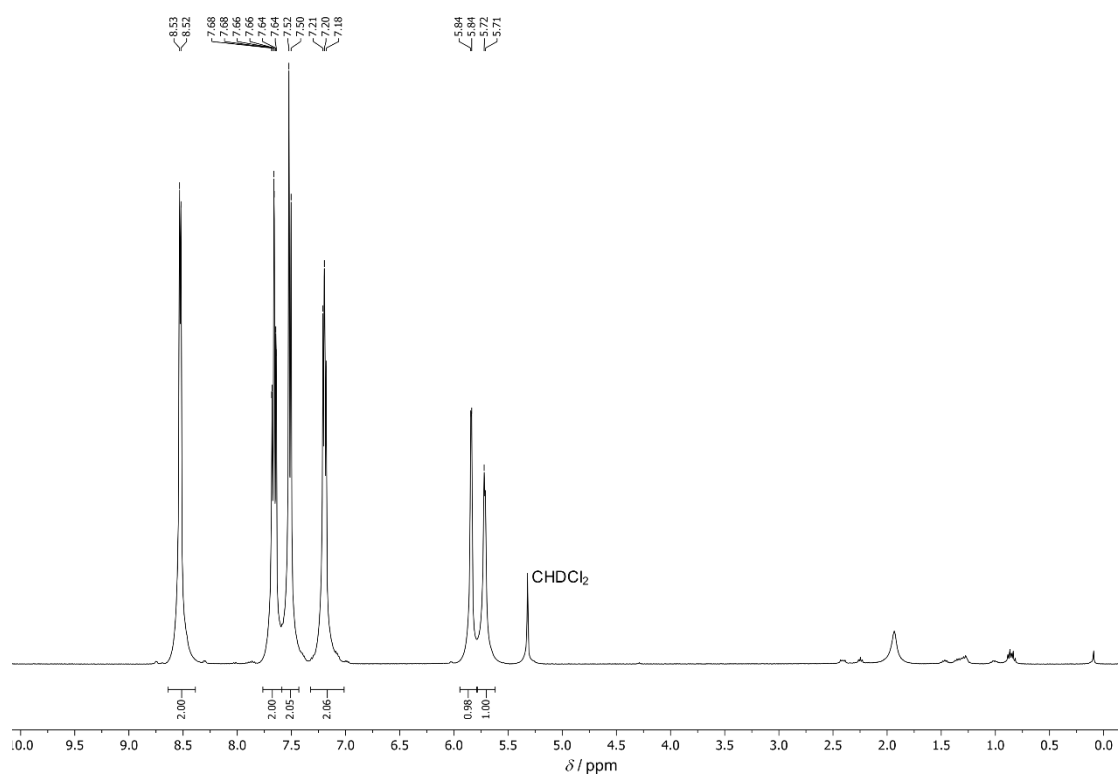
Spectroscopic data
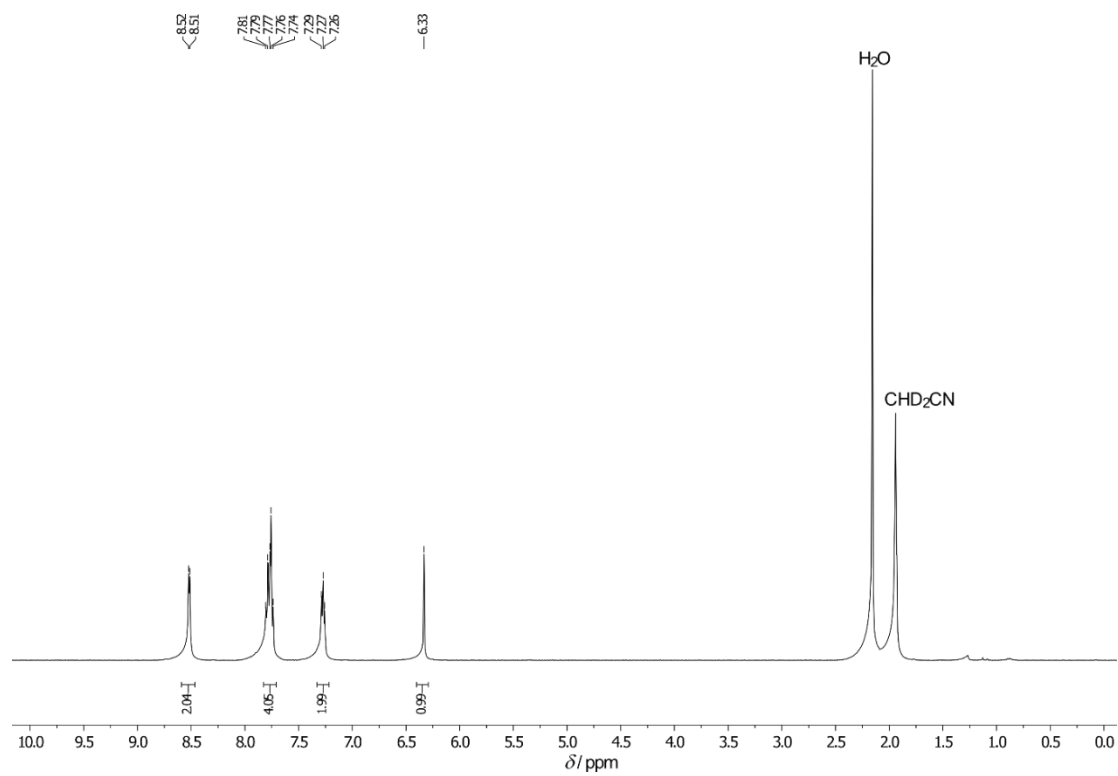

Fig. S1 – ¹H NMR spectrum of **A** in CD₂Cl₂.

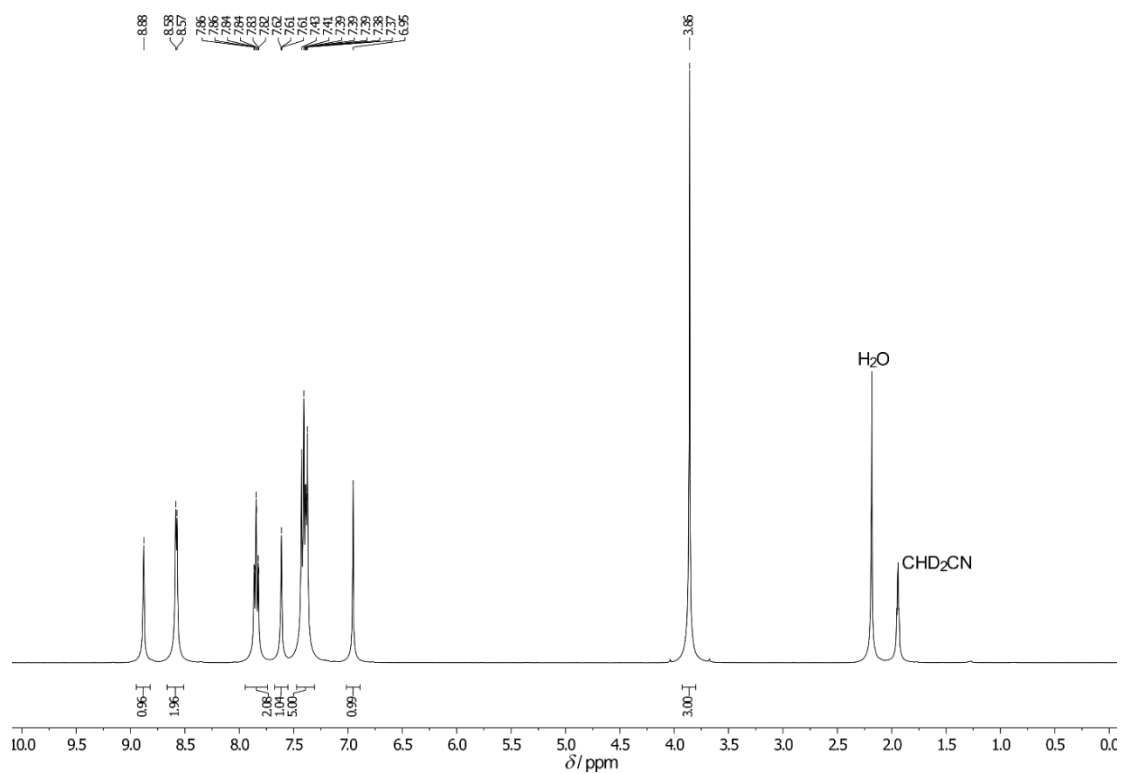

Fig. S2 – ¹H NMR spectrum of **B** in CD₃CN.

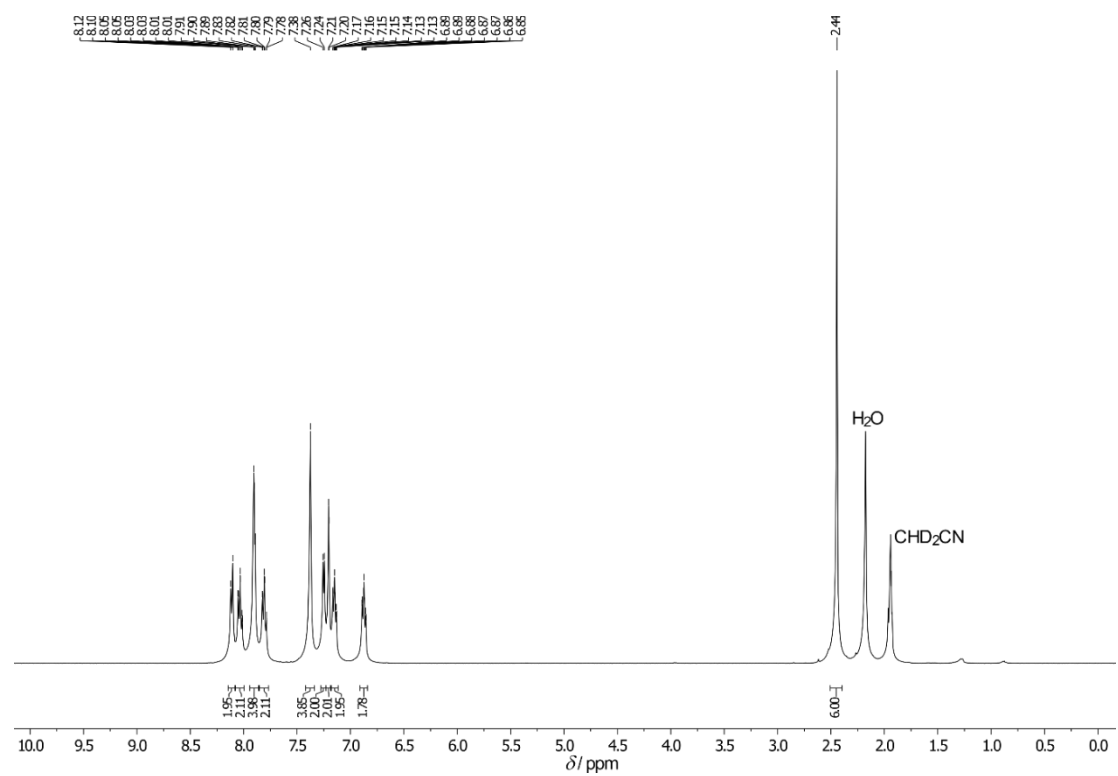**Fig. S3** – ^{1}H NMR spectrum of **C[PF$_6$]** in CD$_3$CN.

Fig. S4 – ^{1}H NMR spectrum of **1[PF$_6$]$_2$** in CD$_3$CN.
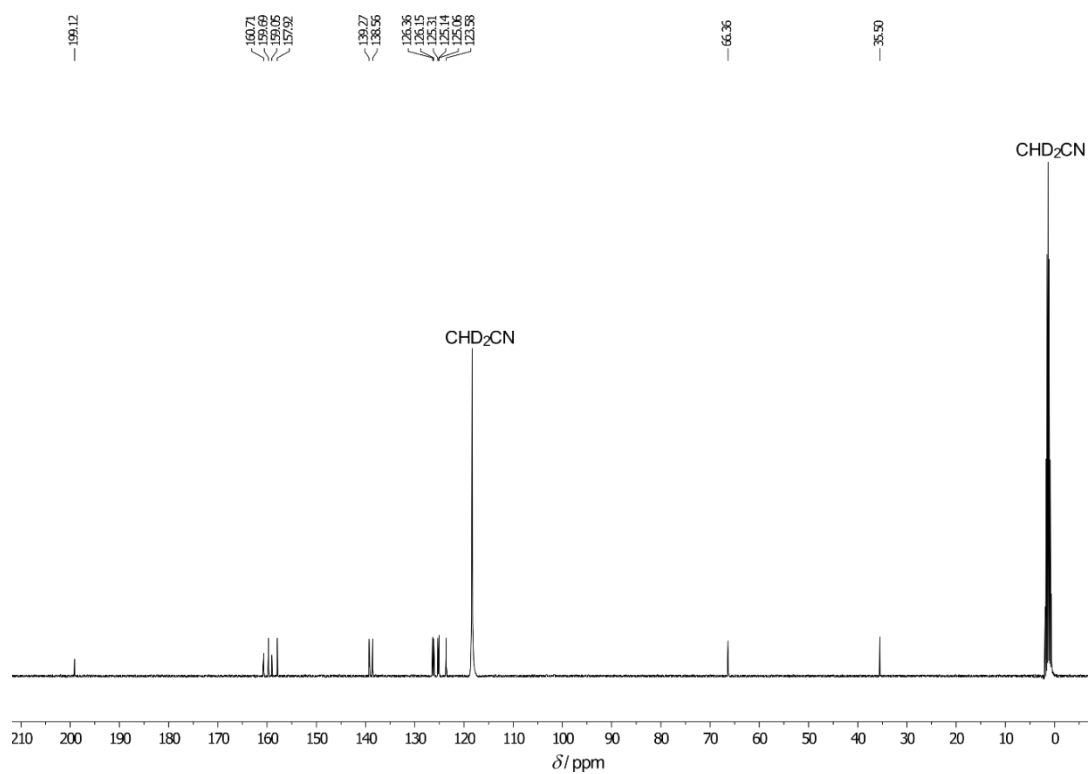
Fig. S5 – $^{13}C\{^1H\}$ NMR spectrum of **1[PF$_6$]$_2$** in CD$_3$CN.
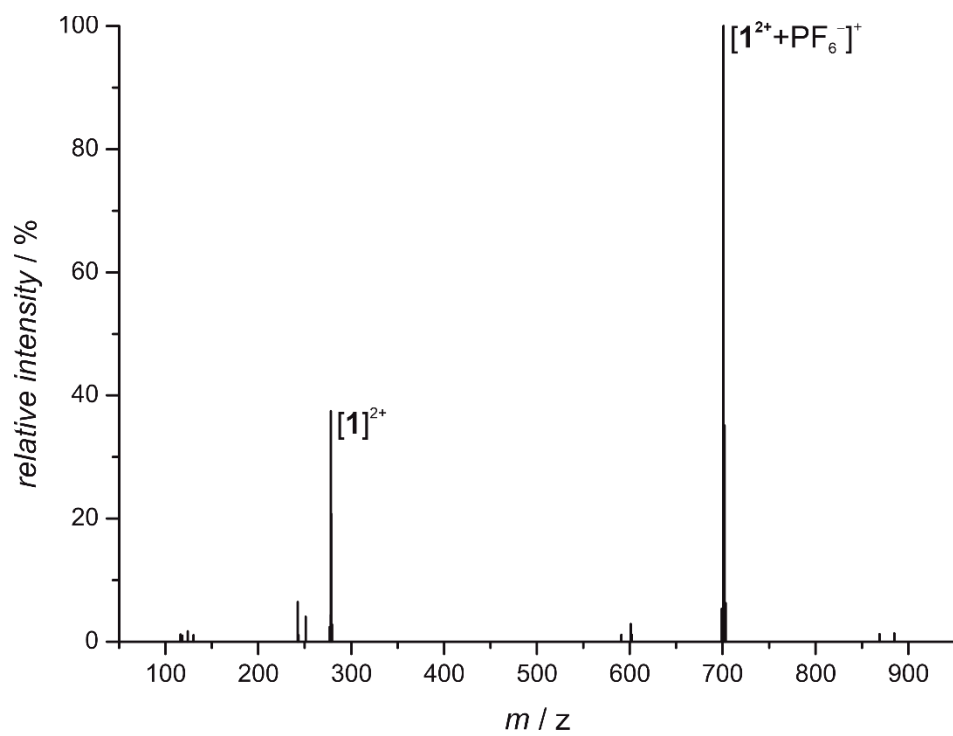
Fig. S6 – ESI$^+$ mass spectrum of **1[PF$_6$]$_2$** in CH$_3$CN.
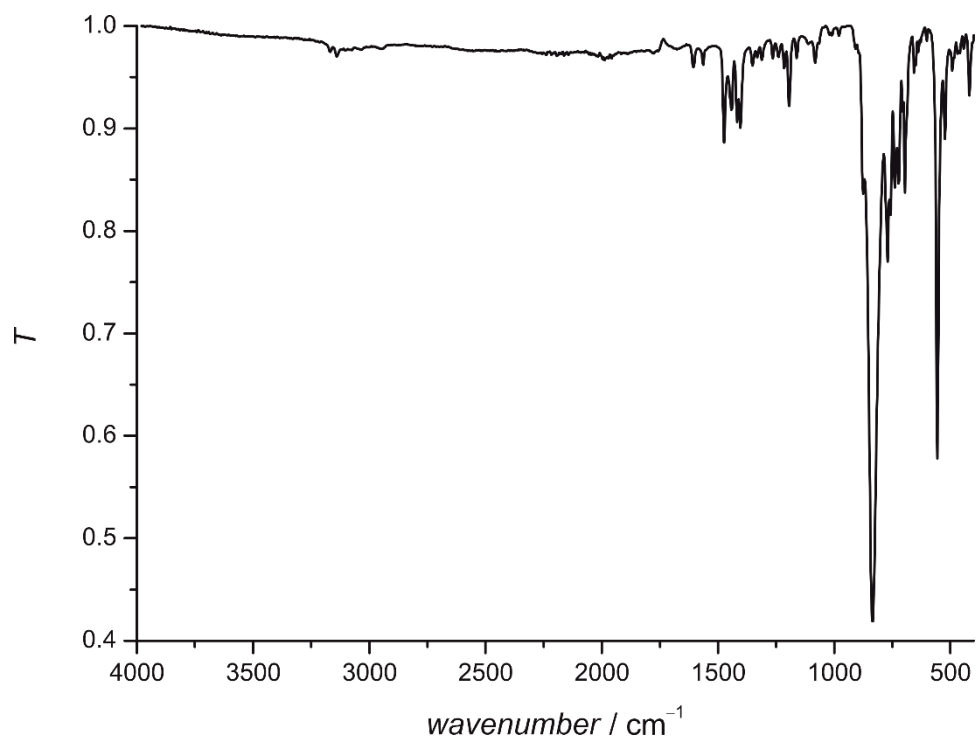
Fig. S7 – ATR IR-spectrum of **1[PF$_6$]$_2$**.

E / V vs. FcH/FcH$^+$
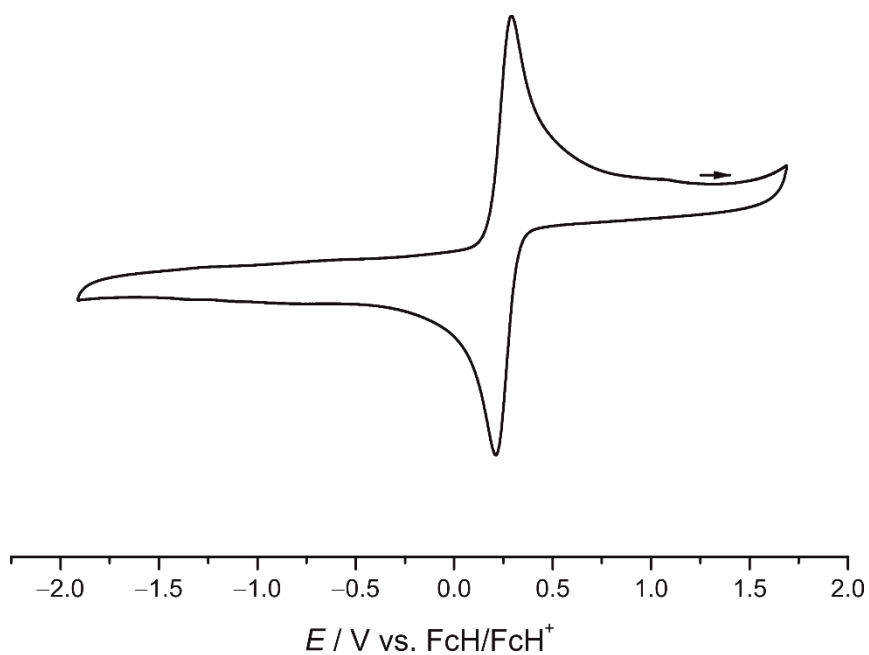
Fig. S8 – Cyclic voltammogramm of **1[PF$_6$]$_2$** in dry, deaerated CH$_3$CN with [^{n}Bu$_4$N][PF$_6$] as supporting electrolyte.
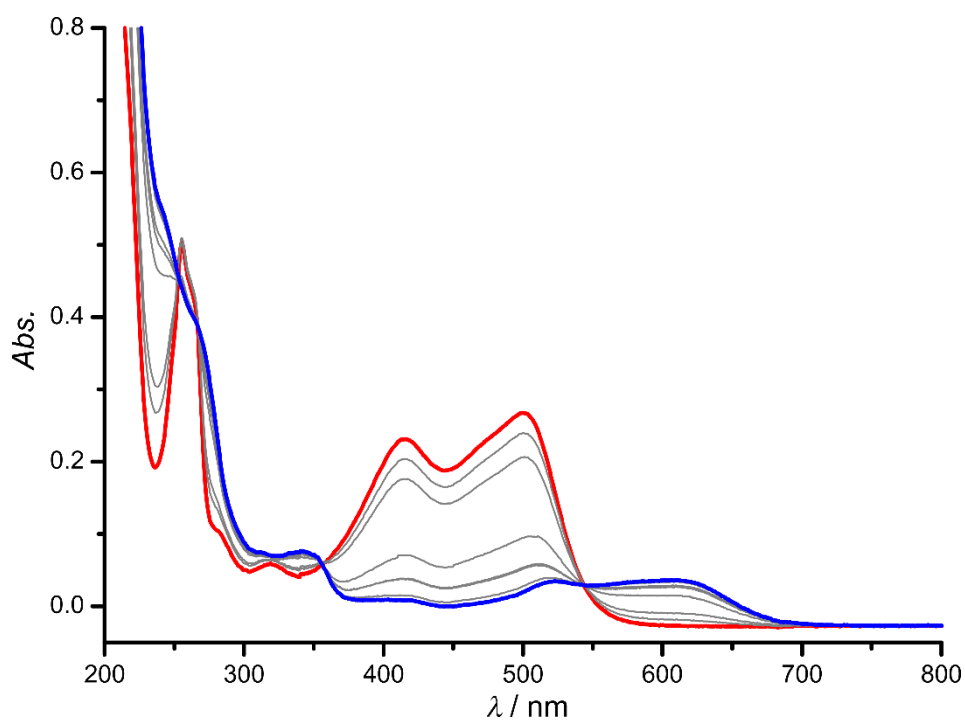
Fig. S9 – Spectroelectrochemical oxidation of **1[PF₆]₂** in CH₃CN with [^{n}Bu₄N][PF₆] as supporting electrolyte (red → blue).
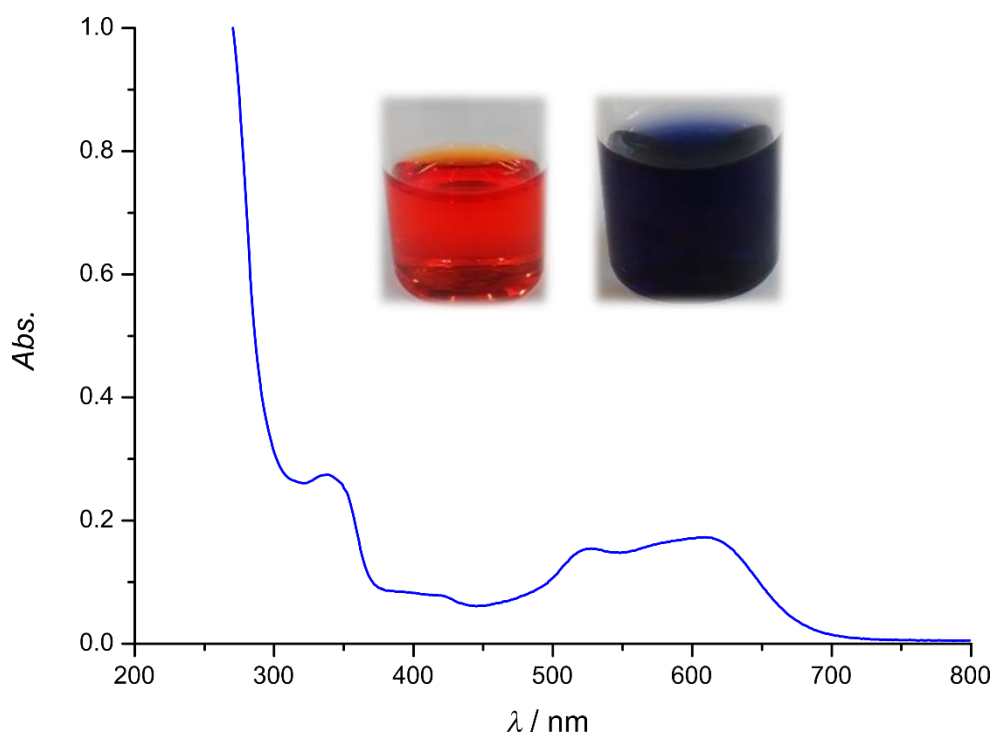
Fig. S10 – UV/Vis spectrum after chemical oxidation of **1[PF₆]₂** with [NO][PF₆] in CH₃CN and photographs of solutions before and after oxidation.
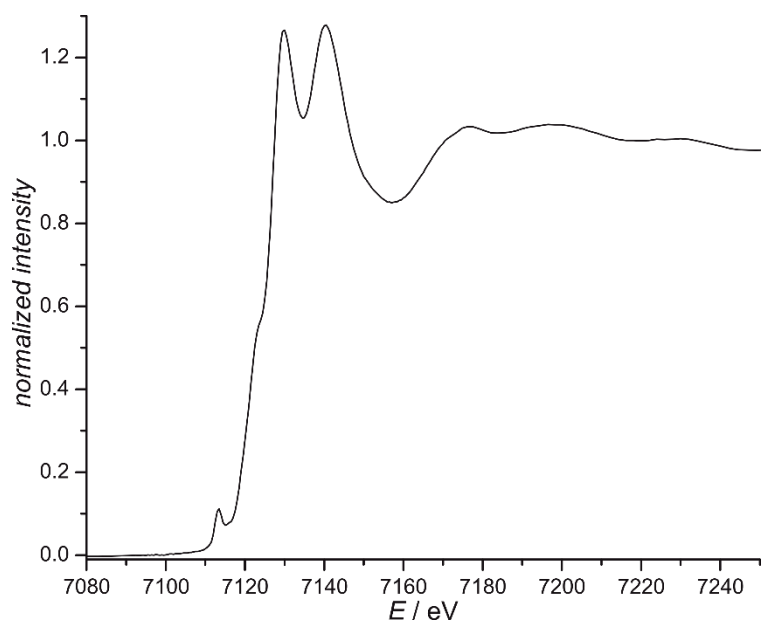
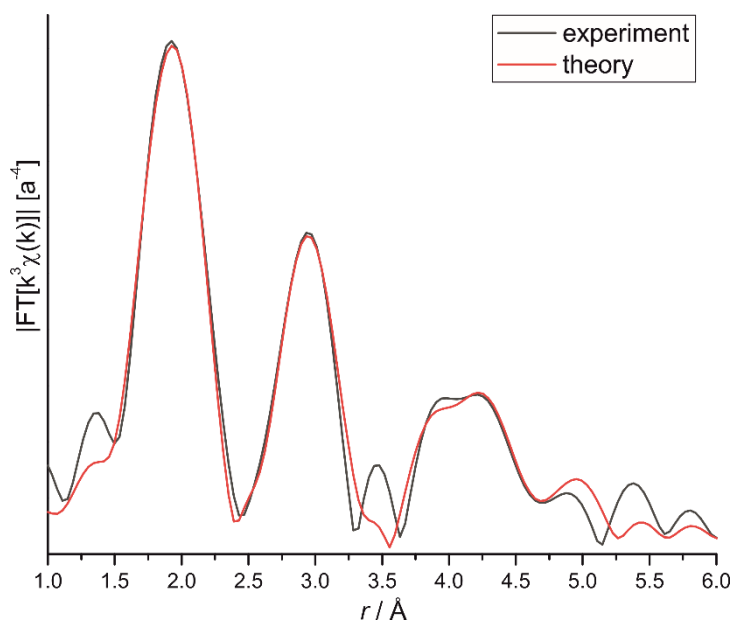**Fig. S11** – XANES spectrum of **1[PF₆]₂**, E_0 = 7121.5 eV.

Fig. S12 – Experimental (black) and theoretical (red) EXAFS fit of **1[PF₆]₂** after Fourier transformation.

Table S1 – Neighbour atoms, coordination numbers and distances of EXAFS analysis for **1[PF₆]₂**.

| Abs-Bs[a]	N(Bs)[b]	R(Abs-Bs) [Å][c]	σ [Å⁻¹][d]	R [%][e] χ^2_{red}[f] E_f[g] Afac[h]
N/C	6.0	1.990	0.084	26.28
N	3.8	2.792	0.039	23.9932E−6
C	5.0	2.927	0.032	5.246
C	8.2	3.853	0.112	0.888
C	5.7	4.378	0.067	
C	3.0	4.852	0.032	
[a] Abs: X-ray absorbing atom, Bs: backscattering atom; [b] Number of backscattering atoms; [c] Distance of absorbing atom to backscattering atom; [d] Debye-Waller like factor; [e] Fit index; [f] Reduced χ^2; [g] Fermi energy, which accounts for the shift between theory and experiment; [h] Amplitude reducing factor.				

Quantum chemical analyses
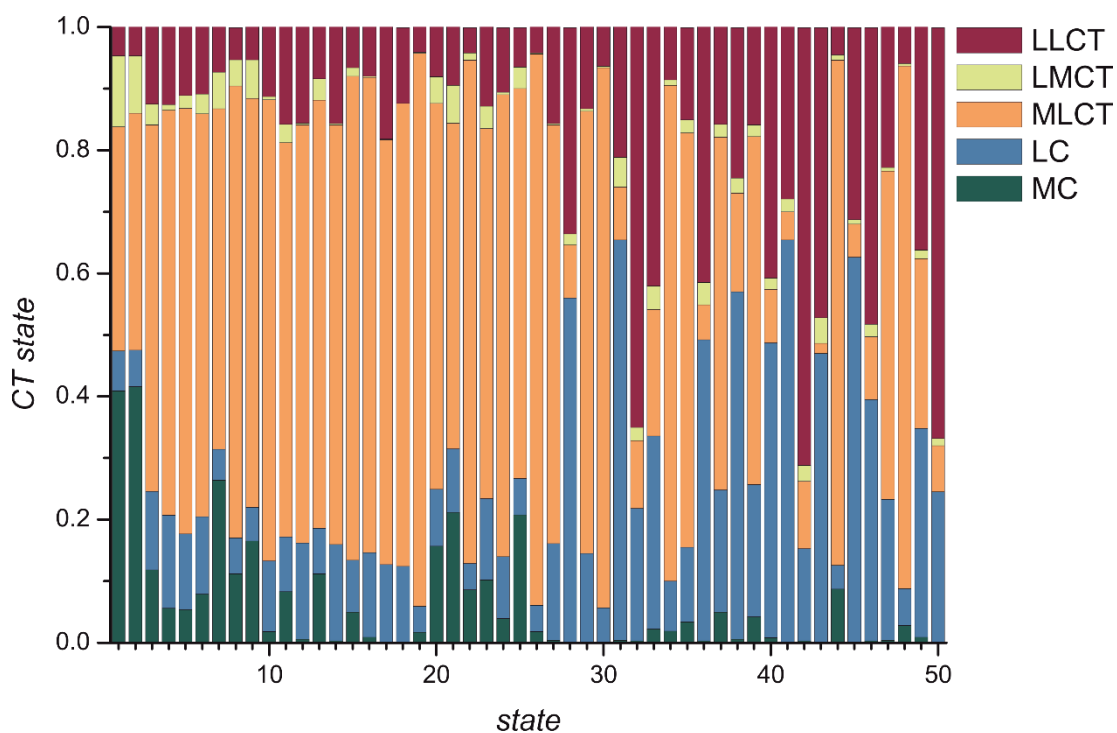
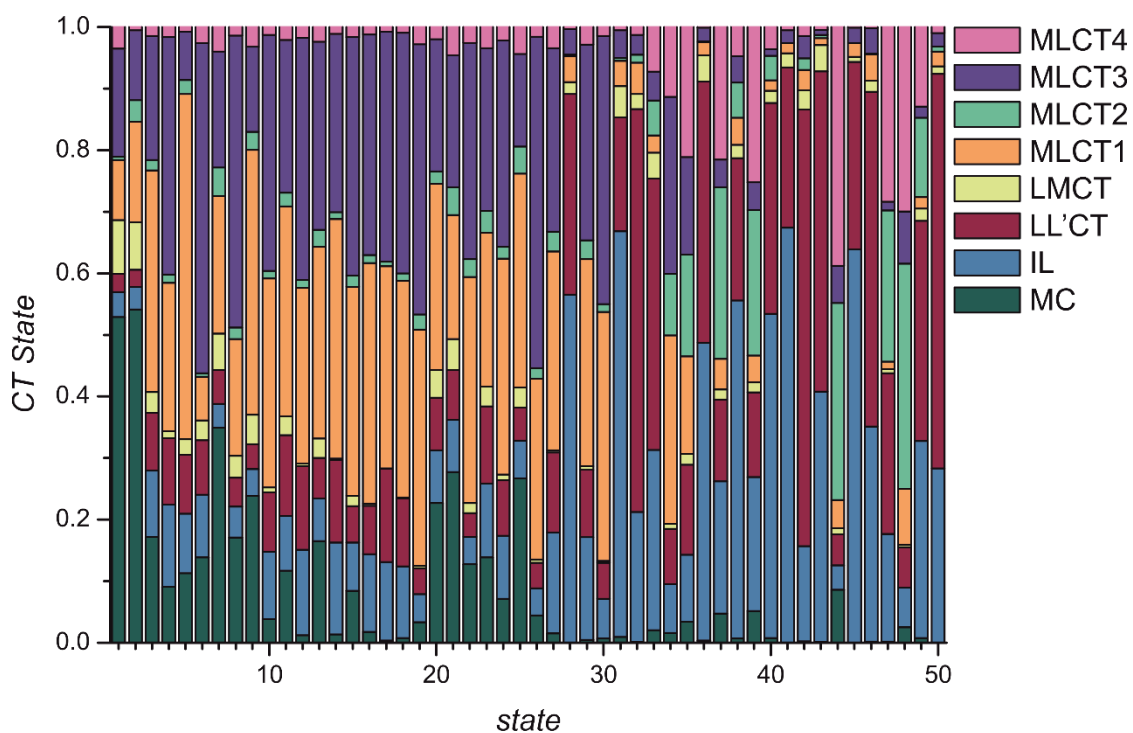**Fig. S13** – Charge transfer number analysis for 1^{2+} from TD-DFT calculation.
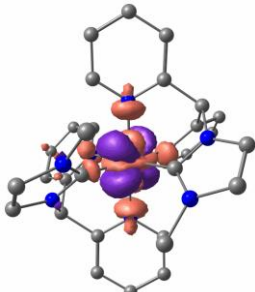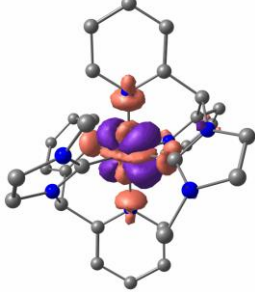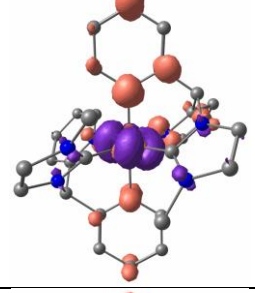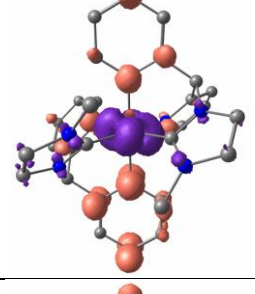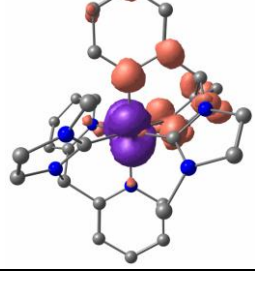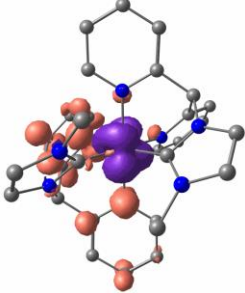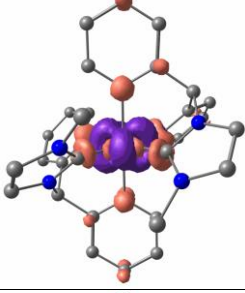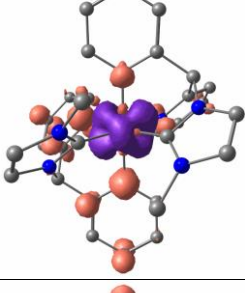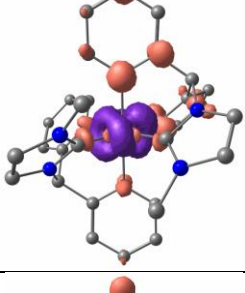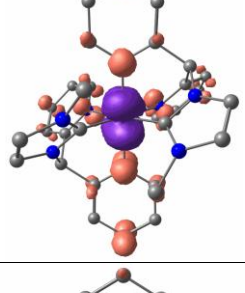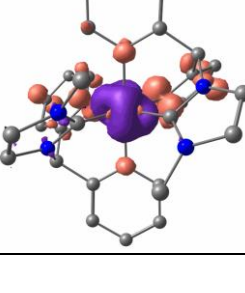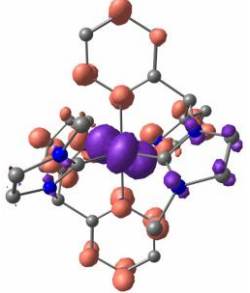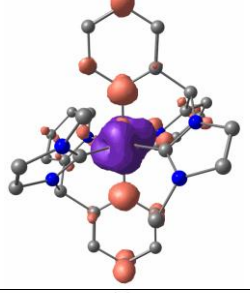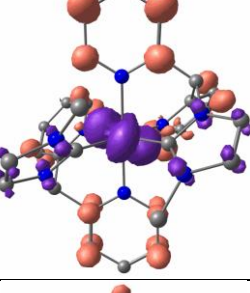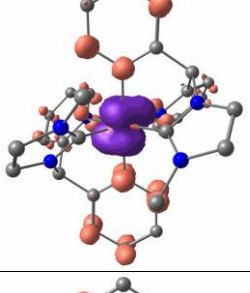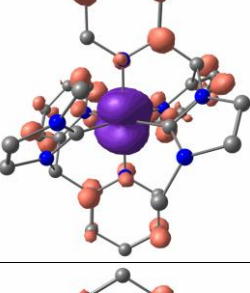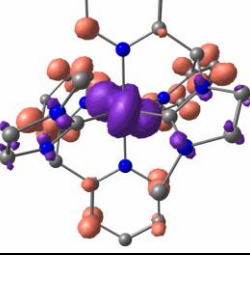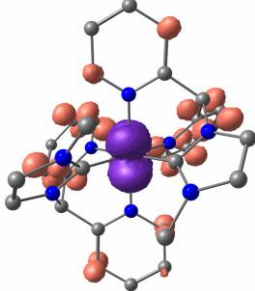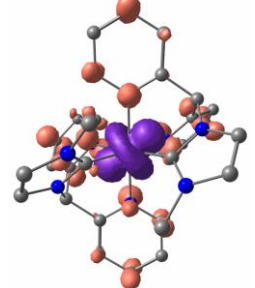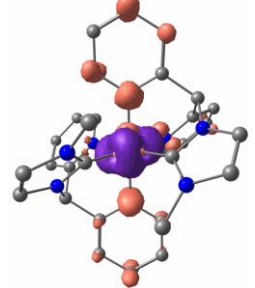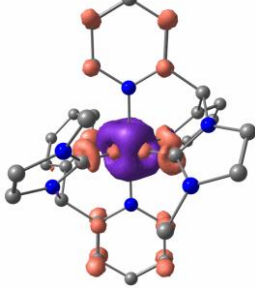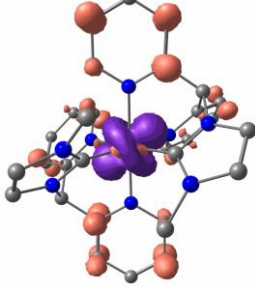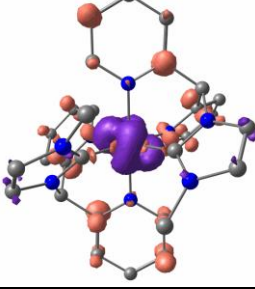
Fig. S14 – Detailed charge transfer number analysis of 1^{2+}; MLCT1: charge transfer from iron to the pyridine moieties of ligand 1, MLCT2: charge transfer from iron to the NHC of ligand 1, MLCT3: charge transfer from iron to the pyridine moieties of ligand 2, MLCT4: charge transfer from iron to the NHC of ligand 2. LMCT: charge transfer from pyridine and carbene moieties to iron, LL'CT: charge transfer from the ligand fragments of ligand 1 to the fragments of ligand 2 or vice versa.
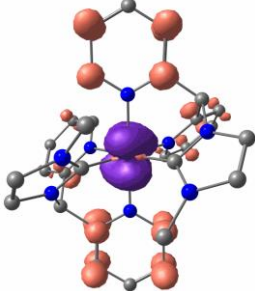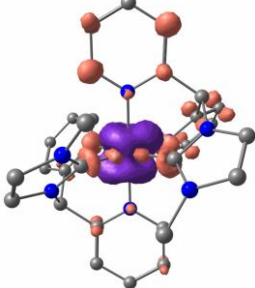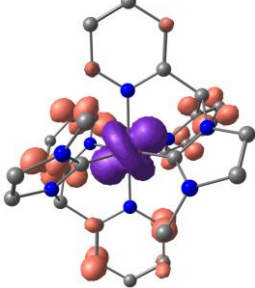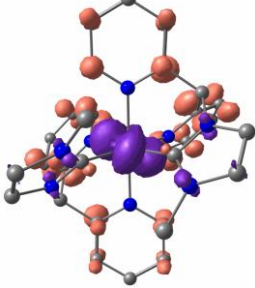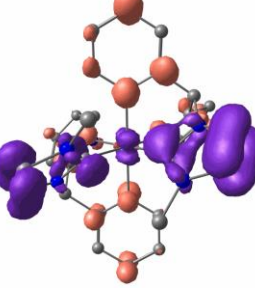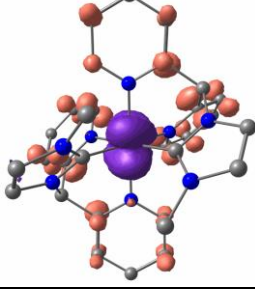
Table S2 – TD-DFT calculated transitions of **1²⁺** with detailed charge transfer number analysis of the transitions; MC = metal centred, LC = ligand centred, LL'CT = ligand-to-ligand charge transfer, LMCT = ligand-to-metal charge transfer, MLCT1 = metal-to-ligand charge transfer from iron to the pyridines of ligand 1, MLCT2 = metal-to-ligand charge transfer from iron to the NHC of ligand 1, MLCT3 = metal-to-ligand charge transfer from iron to the pyridines of ligand 2, MLCT4 = metal-to-ligand charge transfer from iron to the NHC of ligand 2.
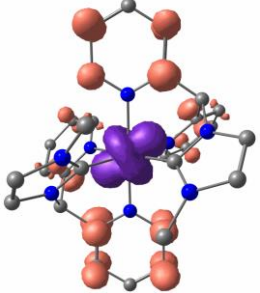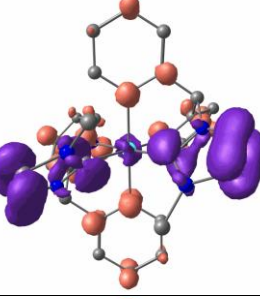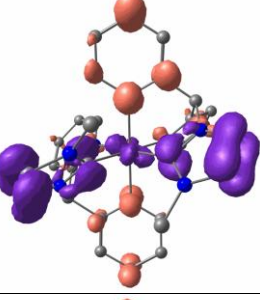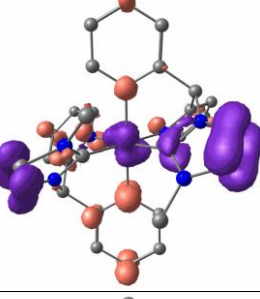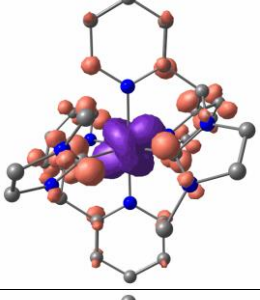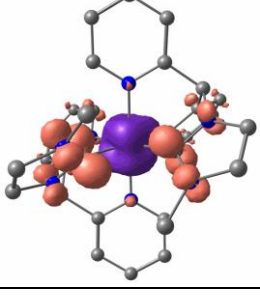
difference density (isosurface value 0.003)	transition number	composition
	1	MC d_{Fe}-d_{Fe} (52.90 %) LC p_L-p_L (4.06 %) LL'CT p_{L1}-p_{L2} (2.93 %) LMCT p_L-d_{Fe} (8.74 %) MLCT1 d_{Fe}-p_{L1-pyr} (9.77 %) MLCT2 d_{Fe}-$p_{L1-carb}$ (0.54 %) MLCT3 d_{Fe}-p_{L2-pyr} (17.57 %) MLCT4 d_{Fe}-$p_{L2-carb}$ (3.49 %)
	2	MC d_{Fe}-d_{Fe} (54.15 %) LC p_L-p_L (3.63 %) LL'CT p_{L1}-p_{L2} (2.81 %) LMCT p_L-d_{Fe} (7.67 %) MLCT1 d_{Fe}-p_{L1-pyr} (16.37 %) MLCT2 d_{Fe}-$p_{L1-carb}$ (3.49 %) MLCT3 d_{Fe}-p_{L2-pyr} (11.35 %) MLCT4 d_{Fe}-$p_{L2-carb}$ (0.53 %)
	3	MC d_{Fe}-d_{Fe} (17.18 %) LC p_L-p_L (10.79 %) LL'CT p_{L1}-p_{L2} (9.36 %) LMCT p_L-d_{Fe} (3.37 %) MLCT1 d_{Fe}-p_{L1-pyr} (36.00 %) MLCT2 d_{Fe}-$p_{L1-carb}$ (1.69 %) MLCT3 d_{Fe}-p_{L2-pyr} (20.14 %) MLCT4 d_{Fe}-$p_{L2-carb}$ (1.48 %)
	4	MC d_{Fe}-d_{Fe} (9.04 %) LC p_L-p_L (13.38 %) LL'CT p_{L1}-p_{L2} (10.84 %) LMCT p_L-d_{Fe} (1.11 %) MLCT1 d_{Fe}-p_{L1-pyr} (24.10 %) MLCT2 d_{Fe}-$p_{L1-carb}$ (1.32 %) MLCT3 d_{Fe}-p_{L2-pyr} (38.54 %) MLCT4 d_{Fe}-$p_{L2-carb}$ (1.67 %)
	5	MC d_{Fe}-d_{Fe} (11.28 %) LC p_L-p_L (9.69 %) LL'CT p_{L1}-p_{L2} (9.61 %) LMCT p_L-d_{Fe} (2.48 %) MLCT1 d_{Fe}-p_{L1-pyr} (56.07 %) MLCT2 d_{Fe}-$p_{L1-carb}$ (2.25 %) MLCT3 d_{Fe}-p_{L2-pyr} (7.89 %) MLCT4 d_{Fe}-$p_{L2-carb}$ (0.73 %)
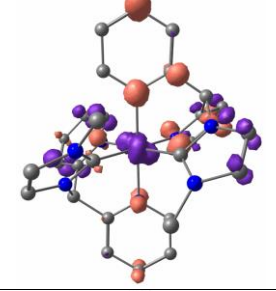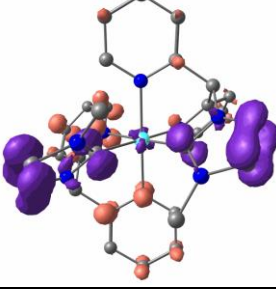
	6	MC d_{Fe}-d_{Fe} (13.86 %) LC p_L-p_L (10.18 %) LL'CT p_{L1}-p_{L2} (8.84 %) LMCT p_L-d_{Fe} (3.21 %) MLCT1 d_{Fe}-$p_{L1\text{-}pyr}$ (7.11 %) MLCT2 d_{Fe}-$p_{L1\text{-}carb}$ (0.56 %) MLCT3 d_{Fe}-$p_{L2\text{-}pyr}$ (53.60 %) MLCT4 d_{Fe}-$p_{L2\text{-}carb}$ (2.64 %)
	7	MC d_{Fe}-d_{Fe} (34.95 %) LC p_L-p_L (3.87 %) LL'CT p_{L1}-p_{L2} (5.45 %) LMCT p_L-d_{Fe} (5.93 %) MLCT1 d_{Fe}-$p_{L1\text{-}pyr}$ (22.34 %) MLCT2 d_{Fe}-$p_{L1\text{-}carb}$ (4.62 %) MLCT3 d_{Fe}-$p_{L2\text{-}pyr}$ (18.83 %) MLCT4 d_{Fe}-$p_{L2\text{-}carb}$ (4.01 %)
	8	MC d_{Fe}-d_{Fe} (17.10 %) LC p_L-p_L (5.03 %) LL'CT p_{L1}-p_{L2} (4.70 %) LMCT p_L-d_{Fe} (3.57 %) MLCT1 d_{Fe}-$p_{L1\text{-}pyr}$ (18.93 %) MLCT2 d_{Fe}-$p_{L1\text{-}carb}$ (1.90 %) MLCT3 d_{Fe}-$p_{L2\text{-}pyr}$ (47.41 %) MLCT4 d_{Fe}-$p_{L2\text{-}carb}$ (1.38 %)
	9	MC d_{Fe}-d_{Fe} (23.87 %) LC p_L-p_L (4.34 %) LL'CT p_{L1}-p_{L2} (4.06 %) LMCT p_L-d_{Fe} (4.76 %) MLCT1 d_{Fe}-$p_{L1\text{-}pyr}$ (43.00 %) MLCT2 d_{Fe}-$p_{L1\text{-}carb}$ (2.94 %) MLCT3 d_{Fe}-$p_{L2\text{-}pyr}$ (13.82 %) MLCT4 d_{Fe}-$p_{L2\text{-}carb}$ (3.21 %)
	10	MC d_{Fe}-d_{Fe} (3.89 %) LC p_L-p_L (10.92 %) LL'CT p_{L1}-p_{L2} (9.57 %) LMCT p_L-d_{Fe} (0.82 %) MLCT1 d_{Fe}-$p_{L1\text{-}pyr}$ (33.97 %) MLCT2 d_{Fe}-$p_{L1\text{-}carb}$ (1.23 %) MLCT3 d_{Fe}-$p_{L2\text{-}pyr}$ (38.33 %) MLCT4 d_{Fe}-$p_{L2\text{-}carb}$ (1.28 %)
	11	MC d_{Fe}-d_{Fe} (11.68 %) LC p_L-p_L (8.90 %) LL'CT p_{L1}-p_{L2} (13.14 %) LMCT p_L-d_{Fe} (3.05 %) MLCT1 d_{Fe}-$p_{L1\text{-}pyr}$ (34.12 %) MLCT2 d_{Fe}-$p_{L1\text{-}carb}$ (2.19 %) MLCT3 d_{Fe}-$p_{L2\text{-}pyr}$ (24.85 %) MLCT4 d_{Fe}-$p_{L2\text{-}carb}$ (2.08 %)
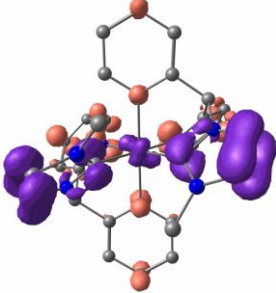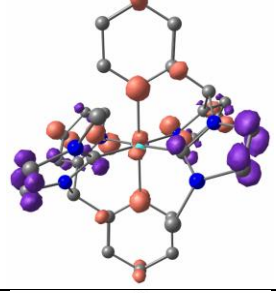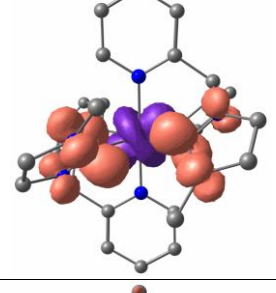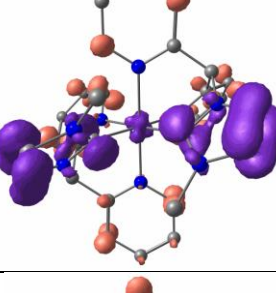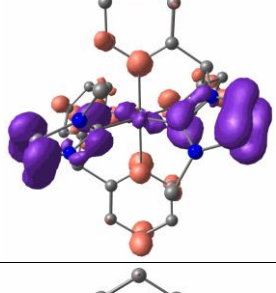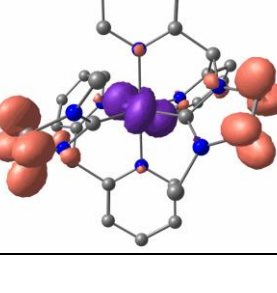
	12	MC d_{Fe}-d_{Fe} (1.26 %) LC p_L-p_L (13.81 %) LL'CT p_{L1}-p_{L2} (13.62 %) LMCT p_L-d_{Fe} (0.39 %) MLCT1 d_{Fe}-$p_{L1\text{-}pyr}$ (28.56 %) MLCT2 d_{Fe}-$p_{L1\text{-}carb}$ (1.28 %) MLCT3 d_{Fe}-$p_{L2\text{-}pyr}$ (39.34 %) MLCT4 d_{Fe}-$p_{L2\text{-}carb}$ (1.75 %)
	13	MC d_{Fe}-d_{Fe} (16.49 %) LC p_L-p_L (6.98 %) LL'CT p_{L1}-p_{L2} (6.55 %) LMCT p_L-d_{Fe} (3.15 %) MLCT1 d_{Fe}-$p_{L1\text{-}pyr}$ (31.17 %) MLCT2 d_{Fe}-$p_{L1\text{-}carb}$ (2.72 %) MLCT3 d_{Fe}-$p_{L2\text{-}pyr}$ (30.56 %) MLCT4 d_{Fe}-$p_{L2\text{-}carb}$ (2.39 %)
	14	MC d_{Fe}-d_{Fe} (1.34 %) LC p_L-p_L (14.92 %) LL'CT p_{L1}-p_{L2} (13.39 %) LMCT p_L-d_{Fe} (0.28 %) MLCT1 d_{Fe}-$p_{L1\text{-}pyr}$ (38.90 %) MLCT2 d_{Fe}-$p_{L1\text{-}carb}$ (1.10 %) MLCT3 d_{Fe}-$p_{L2\text{-}pyr}$ (28.97 %) MLCT4 d_{Fe}-$p_{L2\text{-}carb}$ (1.11 %)
	15	MC d_{Fe}-d_{Fe} (8.45 %) LC p_L-p_L (7.83 %) LL'CT p_{L1}-p_{L2} (5.92 %) LMCT p_L-d_{Fe} (1.66 %) MLCT1 d_{Fe}-$p_{L1\text{-}pyr}$ (33.97 %) MLCT2 d_{Fe}-$p_{L1\text{-}carb}$ (1.82 %) MLCT3 d_{Fe}-$p_{L2\text{-}pyr}$ (38.69 %) MLCT4 d_{Fe}-$p_{L2\text{-}carb}$ (1.66 %)
	16	MC d_{Fe}-d_{Fe} (1.74 %) LC p_L-p_L (12.66 %) LL'CT p_{L1}-p_{L2} (7.82 %) LMCT p_L-d_{Fe} (0.37 %) MLCT1 d_{Fe}-$p_{L1\text{-}pyr}$ (39.07 %) MLCT2 d_{Fe}-$p_{L1\text{-}carb}$ (1.27 %) MLCT3 d_{Fe}-$p_{L2\text{-}pyr}$ (35.83 %) MLCT4 d_{Fe}-$p_{L2\text{-}carb}$ (1.24 %)
	17	MC d_{Fe}-d_{Fe} (0.38 %) LC p_L-p_L (12.72 %) LL'CT p_{L1}-p_{L2} (15.14 %) LMCT p_L-d_{Fe} (0.10 %) MLCT1 d_{Fe}-$p_{L1\text{-}pyr}$ (32.81 %) MLCT2 d_{Fe}-$p_{L1\text{-}carb}$ (0.77 %) MLCT3 d_{Fe}-$p_{L2\text{-}pyr}$ (37.33 %) MLCT4 d_{Fe}-$p_{L2\text{-}carb}$ (0.75 %)
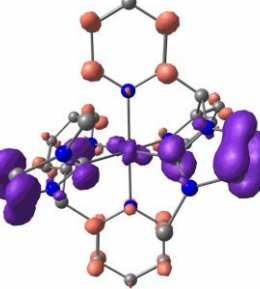
	18	MC d_{Fe}-d_{Fe} (0.78 %) LC p_L-p_L (11.61 %) LL'CT p_{L1}-p_{L2} (11.04 %) LMCT p_L-d_{Fe} (0.16 %) MLCT1 d_{Fe}-$p_{L1\text{-}pyr}$ (35.23 %) MLCT2 d_{Fe}-$p_{L1\text{-}carb}$ (1.14 %) MLCT3 d_{Fe}-$p_{L2\text{-}pyr}$ (39.10 %) MLCT4 d_{Fe}-$p_{L2\text{-}carb}$ (0.95 %)
	19	MC d_{Fe}-d_{Fe} (3.33 %) LC p_L-p_L (4.55 %) LL'CT p_{L1}-p_{L2} (4.16 %) LMCT p_L-d_{Fe} (0.45 %) MLCT1 d_{Fe}-$p_{L1\text{-}pyr}$ (38.36 %) MLCT2 d_{Fe}-$p_{L1\text{-}carb}$ (2.46 %) MLCT3 d_{Fe}-$p_{L2\text{-}pyr}$ (43.90 %) MLCT4 d_{Fe}-$p_{L2\text{-}carb}$ (2.80 %)
	20	MC d_{Fe}-d_{Fe} (22.69 %) LC p_L-p_L (8.55 %) LL'CT p_{L1}-p_{L2} (8.56 %) LMCT p_L-d_{Fe} (4.52 %) MLCT1 d_{Fe}-$p_{L1\text{-}pyr}$ (30.24 %) MLCT2 d_{Fe}-$p_{L1\text{-}carb}$ (2.00 %) MLCT3 d_{Fe}-$p_{L2\text{-}pyr}$ (21.45 %) MLCT4 d_{Fe}-$p_{L2\text{-}carb}$ (1.99 %)
	21	MC d_{Fe}-d_{Fe} (27.71 %) LC p_L-p_L (8.54 %) LL'CT p_{L1}-p_{L2} (8.05 %) LMCT p_L-d_{Fe} (5.03 %) MLCT1 d_{Fe}-$p_{L1\text{-}pyr}$ (20.13 %) MLCT2 d_{Fe}-$p_{L1\text{-}carb}$ (4.49 %) MLCT3 d_{Fe}-$p_{L2\text{-}pyr}$ (21.50 %) MLCT4 d_{Fe}-$p_{L2\text{-}carb}$ (4.56 %)
	22	MC d_{Fe}-d_{Fe} (12.74 %) LC p_L-p_L (4.47 %) LL'CT p_{L1}-p_{L2} (3.85 %) LMCT p_L-d_{Fe} (1.67 %) MLCT1 d_{Fe}-$p_{L1\text{-}pyr}$ (36.68 %) MLCT2 d_{Fe}-$p_{L1\text{-}carb}$ (2.90 %) MLCT3 d_{Fe}-$p_{L2\text{-}pyr}$ (35.11 %) MLCT4 d_{Fe}-$p_{L2\text{-}carb}$ (2.58 %)
	23	MC d_{Fe}-d_{Fe} (13.86 %) LC p_L-p_L (12.00 %) LL'CT p_{L1}-p_{L2} (12.55 %) LMCT p_L-d_{Fe} (3.17 %) MLCT1 d_{Fe}-$p_{L1\text{-}pyr}$ (25.03 %) MLCT2 d_{Fe}-$p_{L1\text{-}carb}$ (3.58 %) MLCT3 d_{Fe}-$p_{L2\text{-}pyr}$ (26.38 %) MLCT4 d_{Fe}-$p_{L2\text{-}carb}$ (3.44 %)

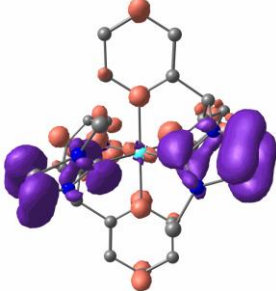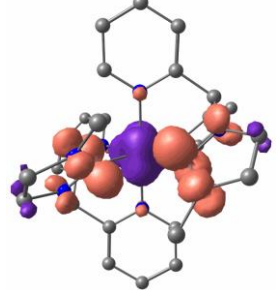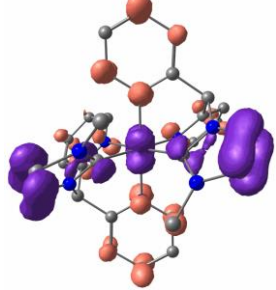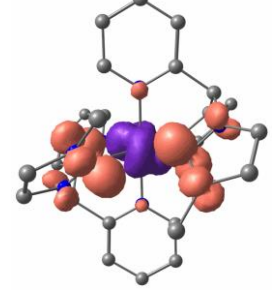|		
	24	MC d_{Fe}-d_{Fe} (7.12 %) LC p_L-p_L (10.27 %) LL'CT p_{L1}-p_{L2} (9.02 %) LMCT p_L-d_{Fe} (0.93 %) MLCT1 d_{Fe}-p_{L1-pyr} (35.01 %) MLCT2 d_{Fe}-$p_{L1-carb}$ (1.97 %) MLCT3 d_{Fe}-p_{L2-pyr} (33.50 %) MLCT4 d_{Fe}-$p_{L2-carb}$ (2.19 %)
	25	MC d_{Fe}-d_{Fe} (26.70 %) LC p_L-p_L (6.13 %) LL'CT p_{L1}-p_{L2} (5.36 %) LMCT p_L-d_{Fe} (3.33 %) MLCT1 d_{Fe}-p_{L1-pyr} (34.66 %) MLCT2 d_{Fe}-$p_{L1-carb}$ (4.41 %) MLCT3 d_{Fe}-p_{L2-pyr} (15.01 %) MLCT4 d_{Fe}-$p_{L2-carb}$ (4.41 %)
	26	MC d_{Fe}-d_{Fe} (4.45 %) LC p_L-p_L (4.40 %) LL'CT p_{L1}-p_{L2} (4.15 %) LMCT p_L-d_{Fe} (0.54 %) MLCT1 d_{Fe}-p_{L1-pyr} (29.36 %) MLCT2 d_{Fe}-$p_{L1-carb}$ (1.72 %) MLCT3 d_{Fe}-p_{L2-pyr} (53.82 %) MLCT4 d_{Fe}-$p_{L2-carb}$ (1.58 %)
	27	MC d_{Fe}-d_{Fe} (1.53 %) LC p_L-p_L (16.39 %) LL'CT p_{L1}-p_{L2} (12.99 %) LMCT p_L-d_{Fe} (0.35 %) MLCT1 d_{Fe}-p_{L1-pyr} (32.28 %) MLCT2 d_{Fe}-$p_{L1-carb}$ (3.25 %) MLCT3 d_{Fe}-p_{L2-pyr} (29.75 %) MLCT4 d_{Fe}-$p_{L2-carb}$ (3.47 %)
	28	MC d_{Fe}-d_{Fe} (0.08 %) LC p_L-p_L (56.44 %) LL'CT p_{L1}-p_{L2} (32.59 %) LMCT p_L-d_{Fe} (1.95 %) MLCT1 d_{Fe}-p_{L1-pyr} (4.20 %) MLCT2 d_{Fe}-$p_{L1-carb}$ (0.23 %) MLCT3 d_{Fe}-p_{L2-pyr} (4.17 %) MLCT4 d_{Fe}-$p_{L2-carb}$ (0.34 %)
	29	MC d_{Fe}-d_{Fe} (0.46 %) LC p_L-p_L (16.70 %) LL'CT p_{L1}-p_{L2} (10.95 %) LMCT p_L-d_{Fe} (0.56 %) MLCT1 d_{Fe}-p_{L1-pyr} (33.66 %) MLCT2 d_{Fe}-$p_{L1-carb}$ (3.05 %) MLCT3 d_{Fe}-p_{L2-pyr} (31.75 %) MLCT4 d_{Fe}-$p_{L2-carb}$ (2.87 %)

	30	MC d_{Fe}-d_{Fe} (0.72 %) LC p_L-p_L (6.43 %) LL'CT p_{L1}-p_{L2} (5.83 %) LMCT p_L-d_{Fe} (0.29 %) MLCT1 d_{Fe}-p_{L1-pyr} (40.44 %) MLCT2 d_{Fe}-$p_{L1-carb}$ (1.28 %) MLCT3 d_{Fe}-p_{L2-pyr} (43.55 %) MLCT4 d_{Fe}-$p_{L2-carb}$ (1.47 %)
	31	MC d_{Fe}-d_{Fe} (0.96 %) LC p_L-p_L (65.87 %) LL'CT p_{L1}-p_{L2} (18.50 %) LMCT p_L-d_{Fe} (5.10 %) MLCT1 d_{Fe}-p_{L1-pyr} (4.08 %) MLCT2 d_{Fe}-$p_{L1-carb}$ (0.45 %) MLCT3 d_{Fe}-p_{L2-pyr} (4.55 %) MLCT4 d_{Fe}-$p_{L2-carb}$ (0.51 %)
	32	MC d_{Fe}-d_{Fe} (0.14 %) LC p_L-p_L (21.12 %) LL'CT p_{L1}-p_{L2} (65.38 %) LMCT p_L-d_{Fe} (2.48 %) MLCT1 d_{Fe}-p_{L1-pyr} (5.06 %) MLCT2 d_{Fe}-$p_{L1-carb}$ (1.32 %) MLCT3 d_{Fe}-p_{L2-pyr} (3.23 %) MLCT4 d_{Fe}-$p_{L2-carb}$ (1.27 %)
	33	MC d_{Fe}-d_{Fe} (2.04 %) LC p_L-p_L (29.24 %) LL'CT p_{L1}-p_{L2} (44.16 %) LMCT p_L-d_{Fe} (4.15 %) MLCT1 d_{Fe}-p_{L1-pyr} (2.76 %) MLCT2 d_{Fe}-$p_{L1-carb}$ (5.68 %) MLCT3 d_{Fe}-p_{L2-pyr} (4.71 %) MLCT4 d_{Fe}-$p_{L2-carb}$ (7.25 %)
	34	MC d_{Fe}-d_{Fe} (1.57 %) LC p_L-p_L (7.98 %) LL'CT p_{L1}-p_{L2} (8.93 %) LMCT p_L-d_{Fe} (0.82 %) MLCT1 d_{Fe}-p_{L1-pyr} (30.63 %) MLCT2 d_{Fe}-$p_{L1-carb}$ (10.00 %) MLCT3 d_{Fe}-p_{L2-pyr} (28.73 %) MLCT4 d_{Fe}-$p_{L2-carb}$ (11.34 %)
	35	MC d_{Fe}-d_{Fe} (3.39 %) LC p_L-p_L (10.91 %) LL'CT p_{L1}-p_{L2} (14.62 %) LMCT p_L-d_{Fe} (1.74 %) MLCT1 d_{Fe}-p_{L1-pyr} (15.87 %) MLCT2 d_{Fe}-$p_{L1-carb}$ (16.48 %) MLCT3 d_{Fe}-p_{L2-pyr} (15.86 %) MLCT4 d_{Fe}-$p_{L2-carb}$ (21.13 %)

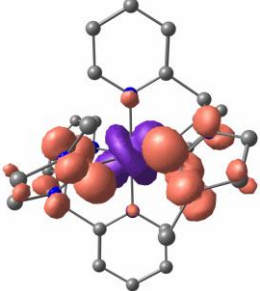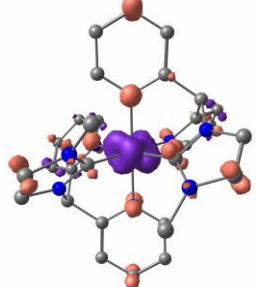|		
	36	MC d_{Fe}-d_{Fe} (0.38 %) LC p_L-p_L (48.37 %) LL'CT p_{L1}-p_{L2} (42.45 %) LMCT p_L-d_{Fe} (4.23 %) MLCT1 d_{Fe}-p_{L1-pyr} (2.13 %) MLCT2 d_{Fe}-$p_{L1-carb}$ (0.11 %) MLCT3 d_{Fe}-p_{L2-pyr} (2.20 %) MLCT4 d_{Fe}-$p_{L2-carb}$ (0.14 %)
	37	MC d_{Fe}-d_{Fe} (4.74 %) LC p_L-p_L (21.49 %) LL'CT p_{L1}-p_{L2} (13.29 %) LMCT p_L-d_{Fe} (1.61 %) MLCT1 d_{Fe}-p_{L1-pyr} (4.97 %) MLCT2 d_{Fe}-$p_{L1-carb}$ (27.89 %) MLCT3 d_{Fe}-p_{L2-pyr} (4.47 %) MLCT4 d_{Fe}-$p_{L2-carb}$ (21.55 %)
	38	MC d_{Fe}-d_{Fe} (0.68 %) LC p_L-p_L (54.93 %) LL'CT p_{L1}-p_{L2} (23.08 %) LMCT p_L-d_{Fe} (2.16 %) MLCT1 d_{Fe}-p_{L1-pyr} (4.42 %) MLCT2 d_{Fe}-$p_{L1-carb}$ (5.70 %) MLCT3 d_{Fe}-p_{L2-pyr} (4.32 %) MLCT4 d_{Fe}-$p_{L2-carb}$ (4.71 %)
	39	MC d_{Fe}-d_{Fe} (5.15 %) LC p_L-p_L (21.74 %) LL'CT p_{L1}-p_{L2} (13.80 %) LMCT p_L-d_{Fe} (1.62 %) MLCT1 d_{Fe}-p_{L1-pyr} (4.30 %) MLCT2 d_{Fe}-$p_{L1-carb}$ (23.64 %) MLCT3 d_{Fe}-p_{L2-pyr} (4.54 %) MLCT4 d_{Fe}-$p_{L2-carb}$ (25.20 %)
	40	MC d_{Fe}-d_{Fe} (0.76 %) LC p_L-p_L (52.67 %) LL'CT p_{L1}-p_{L2} (34.21 %) LMCT p_L-d_{Fe} (2.00 %) MLCT1 d_{Fe}-p_{L1-pyr} (1.71 %) MLCT2 d_{Fe}-$p_{L1-carb}$ (3.98 %) MLCT3 d_{Fe}-p_{L2-pyr} (1.06 %) MLCT4 d_{Fe}-$p_{L2-carb}$ (3.60 %)
	41	MC d_{Fe}-d_{Fe} (0.03 %) LC p_L-p_L (67.39 %) LL'CT p_{L1}-p_{L2} (26.03 %) LMCT p_L-d_{Fe} (2.29 %) MLCT1 d_{Fe}-p_{L1-pyr} (1.64 %) MLCT2 d_{Fe}-$p_{L1-carb}$ (0.05 %) MLCT3 d_{Fe}-p_{L2-pyr} (2.06 %) MLCT4 d_{Fe}-$p_{L2-carb}$ (0.51 %)

	42	MC d_{Fe}-d_{Fe} (0.23 %) LC p_L-p_L (15.46 %) LL'CT p_{L1}-p_{L2} (70.89 %) LMCT p_L-d_{Fe} (3.19 %) MLCT1 d_{Fe}-p_{L1-pyr} (3.28 %) MLCT2 d_{Fe}-$p_{L1-carb}$ (1.83 %) MLCT3 d_{Fe}-p_{L2-pyr} (3.64 %) MLCT4 d_{Fe}-$p_{L2-carb}$ (1.48 %)
	43	MC d_{Fe}-d_{Fe} (0.11 %) LC p_L-p_L (40.65 %) LL'CT p_{L1}-p_{L2} (52.06 %) LMCT p_L-d_{Fe} (4.23 %) MLCT1 d_{Fe}-p_{L1-pyr} (1.11 %) MLCT2 d_{Fe}-$p_{L1-carb}$ (0.53 %) MLCT3 d_{Fe}-p_{L2-pyr} (0.85 %) MLCT4 d_{Fe}-$p_{L2-carb}$ (0.46 %)
	44	MC d_{Fe}-d_{Fe} (8.61 %) LC p_L-p_L (4.00 %) LL'CT p_{L1}-p_{L2} (5.02 %) LMCT p_L-d_{Fe} (1.00 %) MLCT1 d_{Fe}-p_{L1-pyr} (4.56 %) MLCT2 d_{Fe}-$p_{L1-carb}$ (31.97 %) MLCT3 d_{Fe}-p_{L2-pyr} (6.04 %) MLCT4 d_{Fe}-$p_{L2-carb}$ (38.80 %)
	45	MC d_{Fe}-d_{Fe} (0.02 %) LC p_L-p_L (63.87 %) LL'CT p_{L1}-p_{L2} (30.45 %) LMCT p_L-d_{Fe} (0.83 %) MLCT1 d_{Fe}-p_{L1-pyr} (2.20 %) MLCT2 d_{Fe}-$p_{L1-carb}$ (0.08 %) MLCT3 d_{Fe}-p_{L2-pyr} (2.44 %) MLCT4 d_{Fe}-$p_{L2-carb}$ (0.11 %)
	46	MC d_{Fe}-d_{Fe} (0.18 %) LC p_L-p_L (34.95 %) LL'CT p_{L1}-p_{L2} (54.35 %) LMCT p_L-d_{Fe} (1.81 %) MLCT1 d_{Fe}-p_{L1-pyr} (4.28 %) MLCT2 d_{Fe}-$p_{L1-carb}$ (0.13 %) MLCT3 d_{Fe}-p_{L2-pyr} (4.14 %) MLCT4 d_{Fe}-$p_{L2-carb}$ (0.18 %)
	47	MC d_{Fe}-d_{Fe} (0.17 %) LC p_L-p_L (17.53 %) LL'CT p_{L1}-p_{L2} (26.05 %) LMCT p_L-d_{Fe} (0.73 %) MLCT1 d_{Fe}-p_{L1-pyr} (1.18 %) MLCT2 d_{Fe}-$p_{L1-carb}$ (24.56 %) MLCT3 d_{Fe}-p_{L2-pyr} (1.40 %) MLCT4 d_{Fe}-$p_{L2-carb}$ (28.39 %)

	48	MC d_{Fe}-d_{Fe} (2.52 %) LC p_L-p_L (6.42 %) LL'CT p_{L1}-p_{L2} (6.54 %) LMCT p_L-d_{Fe} (0.42 %) MLCT1 d_{Fe}-p_{L1-pyr} (9.07 %) MLCT2 d_{Fe}-$p_{L1-carb}$ (36.62 %) MLCT3 d_{Fe}-p_{L2-pyr} (8.44 %) MLCT4 d_{Fe}-$p_{L2-carb}$ (29.98 %)
	49	MC d_{Fe}-d_{Fe} (0.77 %) LC p_L-p_L (32.02 %) LL'CT p_{L1}-p_{L2} (35.74 %) LMCT p_L-d_{Fe} (1.98 %) MLCT1 d_{Fe}-p_{L1-pyr} (1.84 %) MLCT2 d_{Fe}-$p_{L1-carb}$ (12.89 %) MLCT3 d_{Fe}-p_{L2-pyr} (1.81 %) MLCT4 d_{Fe}-$p_{L2-carb}$ (12.94 %)
	50	MC d_{Fe}-d_{Fe} (0.05 %) LC p_L-p_L (28.26 %) LL'CT p_{L1}-p_{L2} (64.11 %) LMCT p_L-d_{Fe} (1.21 %) MLCT1 d_{Fe}-p_{L1-pyr} (2.38 %) MLCT2 d_{Fe}-$p_{L1-carb}$ (0.86 %) MLCT3 d_{Fe}-p_{L2-pyr} (2.13 %) MLCT4 d_{Fe}-$p_{L2-carb}$ (1.01 %)

Cartesian coordinates of optimised geometries for **1²⁺**

¹GS

26	1.791047000	1.634849000	7.351698000
7	2.852863000	-0.074475000	7.240048000
6	3.467245000	2.602920000	7.384318000
7	1.923161000	1.463772000	9.388851000
6	2.164165000	1.083429000	12.133442000
1	2.258529000	0.924281000	13.199243000
6	4.242478000	0.912739000	8.965198000
6	5.328202000	3.882505000	7.234060000
6	5.605913000	2.887985000	8.107069000
7	4.020158000	3.694427000	6.803881000
6	3.099884000	1.113439000	9.934871000
6	0.950591000	1.458226000	11.573963000
1	0.069169000	1.606294000	12.181550000
6	0.873987000	1.642436000	10.203910000
1	-0.054447000	1.932341000	9.735659000
6	3.258881000	0.913237000	11.295602000
1	4.224741000	0.625937000	11.687331000
1	5.154556000	0.703079000	9.514930000
6	3.922638000	-0.240105000	8.039075000
6	4.679826000	-1.400535000	8.034510000
1	5.533299000	-1.487084000	8.692312000
6	4.324811000	-2.433996000	7.178648000
1	4.898854000	-3.350264000	7.157944000
6	3.223865000	-2.263290000	6.349785000
1	2.906355000	-3.036273000	5.664364000
6	2.519809000	-1.074013000	6.407255000
1	1.659502000	-0.906237000	5.777824000
7	4.454215000	2.123454000	8.180446000
7	0.701829000	3.318551000	7.523808000
7	0.035670000	0.588033000	7.400217000
6	1.569211000	1.753922000	5.430593000
6	-0.762253000	2.303271000	5.882236000
6	-1.351364000	-1.173586000	8.233498000
1	-1.431328000	-2.067749000	8.834537000
6	-2.273950000	0.489621000	6.788242000
1	-3.094909000	0.922830000	6.233720000
6	-2.448220000	-0.649575000	7.563756000
1	-3.417905000	-1.123248000	7.633975000
6	-0.133775000	-0.523804000	8.131142000
1	0.735223000	-0.893467000	8.653612000
7	0.334238000	2.049234000	4.955099000
6	1.550573000	1.763454000	3.167666000
7	2.315003000	1.583171000	4.313729000
6	0.294229000	2.059373000	3.571338000
1	-1.647761000	2.540606000	5.301526000
6	-0.405098000	3.470511000	6.775148000
6	-1.171202000	4.624755000	6.806952000
1	-2.050888000	4.701701000	6.183441000
6	-0.782341000	5.669515000	7.633847000

1	-1.356163000	6.585567000	7.667650000
6	0.357288000	5.512357000	8.411861000
1	0.703587000	6.294989000	9.071881000
6	1.065436000	4.326748000	8.332969000
1	1.957367000	4.171377000	8.920180000
6	-1.019033000	1.070568000	6.721260000
1	-0.600797000	2.274672000	3.016417000
1	1.970108000	1.666346000	2.182280000
6	3.738028000	1.280933000	4.279213000
1	4.103571000	1.192006000	5.294852000
1	3.908764000	0.344698000	3.750378000
1	4.272913000	2.081387000	3.770307000
6	3.365194000	4.588362000	5.861036000
1	3.972103000	4.677593000	4.961689000
1	2.395373000	4.181354000	5.603057000
1	3.236810000	5.572663000	6.310003000
1	6.492775000	2.657449000	8.669089000
1	5.930890000	4.700671000	6.882562000

³MLCT

26	1.758494000	1.579271000	7.381116000
7	2.759472000	-0.030170000	7.247907000
6	3.377435000	2.573524000	7.358939000
7	1.895462000	1.438636000	9.270947000
6	2.065892000	0.976637000	12.021913000
1	2.132943000	0.789952000	13.084861000
6	4.222980000	0.912679000	8.909010000
6	5.160312000	3.933189000	7.172377000
6	5.508646000	2.936862000	8.025537000
7	3.856716000	3.697148000	6.775940000
6	3.063472000	1.084363000	9.854548000
6	0.864184000	1.349608000	11.435743000
1	-0.037133000	1.469138000	12.019704000
6	0.817129000	1.572404000	10.073290000
1	-0.103286000	1.864823000	9.596141000
6	3.185440000	0.842375000	11.207913000
1	4.145678000	0.557895000	11.614495000
1	5.139558000	0.711563000	9.452177000
6	3.887110000	-0.215051000	7.967113000
6	4.675305000	-1.346523000	7.858316000
1	5.569238000	-1.431335000	8.459493000
6	4.299269000	-2.346773000	6.973125000
1	4.900864000	-3.238045000	6.860515000
6	3.137352000	-2.169647000	6.232629000
1	2.792684000	-2.918027000	5.533500000
6	2.405039000	-1.010040000	6.388949000
1	1.497748000	-0.850963000	5.830876000
7	4.398612000	2.129730000	8.119558000
7	0.724616000	3.165895000	7.535127000
7	0.152755000	0.563803000	7.360448000
6	1.640639000	1.717498000	5.489819000

6	-0.702387000	2.230390000	5.824358000
6	-1.312035000	-0.949536000	8.541548000
1	-1.401565000	-1.769277000	9.241097000
6	-2.243380000	0.636406000	7.002494000
1	-3.072379000	1.096839000	6.480359000
6	-2.448977000	-0.388805000	7.924572000
1	-3.441539000	-0.753013000	8.147112000
6	-0.069046000	-0.464590000	8.246725000
1	0.806879000	-0.890123000	8.709386000
7	0.434192000	1.957670000	4.938996000
6	1.763339000	1.659276000	3.239784000
7	2.463890000	1.532427000	4.429755000
6	0.474838000	1.926101000	3.561924000
1	-1.572007000	2.464041000	5.220043000
6	-0.327719000	3.391384000	6.702533000
6	-1.016118000	4.593815000	6.675439000
1	-1.837948000	4.714212000	5.982572000
6	-0.635362000	5.618227000	7.524159000
1	-1.142337000	6.572599000	7.501624000
6	0.421790000	5.382611000	8.410292000
1	0.752804000	6.137898000	9.108798000
6	1.063867000	4.167892000	8.385848000
1	1.890806000	3.974206000	9.050355000
6	-0.964236000	1.069514000	6.727590000
1	-0.393355000	2.092850000	2.950571000
1	2.244636000	1.548749000	2.284672000
6	3.902276000	1.293491000	4.458023000
1	4.216010000	1.045918000	5.463601000
1	4.141101000	0.465328000	3.795044000
1	4.430795000	2.184969000	4.123066000
6	3.122476000	4.617180000	5.913154000
1	3.801221000	5.009778000	5.160939000
1	2.308645000	4.093310000	5.427445000
1	2.721519000	5.437616000	6.505579000
1	6.421048000	2.735908000	8.556884000
1	5.717126000	4.780263000	6.814181000

³MC

26	1.767853000	1.630782000	7.386372000
7	2.966404000	-0.386515000	7.304323000
6	3.496822000	2.561828000	7.465891000
7	1.971113000	1.397752000	9.414839000
6	2.192470000	0.823864000	12.125345000
1	2.280503000	0.588330000	13.177293000
6	4.290633000	0.777525000	8.972410000
6	5.391681000	3.781558000	7.307758000
6	5.660104000	2.738692000	8.126587000
7	4.067549000	3.655548000	6.914634000
6	3.129861000	0.947612000	9.926959000
6	1.005811000	1.317398000	11.601968000
1	0.139348000	1.487618000	12.225040000

6	0.936129000	1.587971000	10.246928000
1	0.028130000	1.964446000	9.800361000
6	3.271876000	0.643523000	11.271325000
1	4.219439000	0.275497000	11.639471000
1	5.194244000	0.613960000	9.551657000
6	4.083417000	-0.403874000	8.035793000
6	5.015374000	-1.427340000	7.942950000
1	5.910632000	-1.408471000	8.549096000
6	4.771866000	-2.465577000	7.050636000
1	5.481033000	-3.276780000	6.951370000
6	3.611371000	-2.443983000	6.287958000
1	3.383787000	-3.231818000	5.583527000
6	2.735170000	-1.379646000	6.444963000
1	1.820377000	-1.314083000	5.869030000
7	4.487155000	2.009277000	8.208144000
7	0.396116000	3.532945000	7.635187000
7	-0.031731000	0.628755000	7.405255000
6	1.491540000	1.784859000	5.451776000
6	-0.851884000	2.371754000	5.902158000
6	-1.456572000	-1.049855000	8.337118000
1	-1.547610000	-1.938927000	8.944009000
6	-2.375886000	0.662573000	6.947453000
1	-3.206371000	1.140057000	6.446077000
6	-2.563825000	-0.458624000	7.744239000
1	-3.553434000	-0.870740000	7.888137000
6	-0.213633000	-0.472284000	8.149574000
1	0.669338000	-0.887791000	8.611071000
7	0.257397000	2.099558000	4.989747000
6	1.459864000	1.788527000	3.193109000
7	2.228397000	1.605497000	4.333447000
6	0.210833000	2.104566000	3.606233000
1	-1.734691000	2.540743000	5.293088000
6	-0.568021000	3.625639000	6.715326000
6	-1.251333000	4.807609000	6.472302000
1	-2.023492000	4.847403000	5.716081000
6	-0.908692000	5.935537000	7.208266000
1	-1.413171000	6.875405000	7.028239000
6	0.094039000	5.839226000	8.164776000
1	0.393884000	6.693156000	8.755729000
6	0.720024000	4.614053000	8.346200000
1	1.513251000	4.491195000	9.073931000
6	-1.095890000	1.169444000	6.786686000
1	-0.683859000	2.333644000	3.056254000
1	1.869378000	1.678099000	2.204911000
6	3.641426000	1.257742000	4.304266000
1	4.025868000	1.282831000	5.316903000
1	3.776525000	0.258207000	3.893368000
1	4.182299000	1.975325000	3.690228000
6	3.397393000	4.610223000	6.044933000
1	3.972557000	4.734747000	5.129374000
1	2.410285000	4.232346000	5.804739000
1	3.304861000	5.570877000	6.549710000

| 1 | 6.556875000 | 2.451730000 | 8.645242000 |
| 1 | 6.011282000 | 4.594797000 | 6.974781000 |

⁵MC

26	1.898810000	1.699650000	7.216122000
7	3.032784000	-0.232064000	7.318343000
6	3.801741000	2.624429000	7.463095000
7	1.991634000	1.450627000	9.496730000
6	2.222286000	1.140802000	12.240219000
1	2.317093000	1.017233000	13.310733000
6	4.324063000	0.837557000	9.099706000
6	5.730812000	3.792920000	7.580493000
6	5.841587000	2.754834000	8.442369000
7	4.479737000	3.689757000	6.994259000
6	3.157175000	1.077951000	10.040322000
6	1.018177000	1.537010000	11.675744000
1	0.146154000	1.732024000	12.283702000
6	0.948413000	1.679398000	10.298638000
1	0.028880000	1.981401000	9.815923000
6	3.310952000	0.909462000	11.408574000
1	4.266890000	0.606103000	11.812445000
1	5.196870000	0.600221000	9.700268000
6	4.068411000	-0.330238000	8.162359000
6	4.888907000	-1.447801000	8.190761000
1	5.716139000	-1.495488000	8.885164000
6	4.631717000	-2.491623000	7.309895000
1	5.260123000	-3.372143000	7.309390000
6	3.562976000	-2.383968000	6.431532000
1	3.328108000	-3.171036000	5.729138000
6	2.787910000	-1.234967000	6.471211000
1	1.941740000	-1.103979000	5.809173000
7	4.652317000	2.053069000	8.347840000
7	0.542153000	3.471153000	7.441577000
7	-0.116521000	0.588665000	7.368112000
6	1.398615000	1.798026000	5.146636000
6	-0.919419000	2.326633000	5.849430000
6	-1.501432000	-1.184694000	8.169157000
1	-1.591439000	-2.078088000	8.770709000
6	-2.404454000	0.474018000	6.701194000
1	-3.220047000	0.897424000	6.131349000
6	-2.581375000	-0.674586000	7.462571000
1	-3.545700000	-1.163515000	7.497338000
6	-0.287076000	-0.519777000	8.093288000
1	0.579372000	-0.878799000	8.632382000
7	0.115048000	2.095144000	4.837182000
6	1.109744000	1.833501000	2.907749000
7	2.000468000	1.645701000	3.951960000
6	-0.089728000	2.116692000	3.468471000
1	-1.834064000	2.551793000	5.309855000
6	-0.588155000	3.521948000	6.725409000
6	-1.445867000	4.610481000	6.783468000

1	-2.353295000	4.618132000	6.195802000
6	-1.114725000	5.682138000	7.603783000
1	-1.766693000	6.543159000	7.665672000
6	0.063587000	5.631968000	8.335278000
1	0.362000000	6.444999000	8.981783000
6	0.863227000	4.505215000	8.223163000
1	1.790048000	4.415957000	8.774712000
6	-1.154500000	1.074674000	6.675988000
1	-1.047054000	2.329257000	3.027252000
1	1.403641000	1.752870000	1.876385000
6	3.407530000	1.311183000	3.783785000
1	3.879817000	1.315612000	4.761658000
1	3.506554000	0.323162000	3.335935000
1	3.889018000	2.048528000	3.143602000
6	3.961847000	4.614289000	5.995533000
1	4.635119000	4.650141000	5.140400000
1	2.986057000	4.261239000	5.675026000
1	3.866781000	5.611582000	6.423011000
1	6.641413000	2.458465000	9.097129000
1	6.420593000	4.580514000	7.334675000

1   G. R. Fulmer, A. J. M. Miller, N. H. Sherden, H. E. Gottlieb, A. Nudelman, B. M. Stoltz, J. E. Bercaw and K. I. Goldberg, *Organometallics*, 2010, **29**, 2176.

2   M. Krejčik, M. Daněk and F.Hartl, *J. Electroanal. Chem.*, 1991, **317**, 179.

3   a) T. S. Ertel, H. Bertagnolli, S. Hückmann, U. Kolb and D. Peter, *Appl. Spectrosc.*, 1992, **46**, 690; b) M. Newville, *J. Synchrotron. Rad.*, 2001, **8**, 322; c) M. Newville, P. Līviņš, Y. Yacoby, J. J. Rehr and E. A. Stern, *Phys. Rev. B*, 1993, **47**, 14126; d) B. Ravel and M. Newville, *J. Synchrotron. Rad.*, 2005, **12**, 537.

4   N. Binsted and S. S. Hasnain, *J. Synchrotron. Rad.*, 1996, **3**, 185.

5   N. Binsted and F. Mosselmans, EXCURV98 Manual, Daresbury, UK.

6   M. Bauer and H. Bertagnolli, *J. Phys. Chem. B*, 2007, **111**, 13756.

7   D. C. Koningsberger, B. L. Mojet, G. E. van Dorssen and D. E. Ramaker, *Top. Catal.*, 2000, **10**, 143.

8   A. Päpcke, A. Friedrich and S. Lochbrunner, *J. Phys.: Condens. Matter*, 2020, **32**, 153001.

9   F. Neese, *WIREs Comput. Mol. Sci.*, 2012, **2**, 73–78.

10   F. Neese, *WIREs Comput. Mol. Sci.*, 2018, **8**, e1327.

11   A. D. Becke, *J. Chem. Phys.*, 1993, **98**, 5648–5652.

12   C. Lee, W. Yang and R. G. Parr, *Phys. Rev. B*, 1988, **37**, 785–789.

13   B. Miehlich, A. Savin, H. Stoll and H. Preuss, *Chem. Phys. Lett.*, 1989, **157**, 200–206.

14   D. A. Pantazis, X.-Y. Chen, C. R. Landis and F. Neese, *J. Chem. Theory Comput.*, 2008, **4**, 908–919.

15   F. Weigend and R. Ahlrichs, *Phys. Chem. Chem. Phys.*, 2005, **7**, 3297–3305.

16   S. Miertuš, E. Scrocco and J. Tomasi, *Chem. Phys.*, 1981, **55**, 117–129.

17   V. Barone and M. Cossi, *J. Phys. Chem. A*, 1998, **102**, 1995–2001.

18   F. Neese, F. Wennmohs, A. Hansen and U. Becker, *Chem. Phys.*, 2009, **356**, 98–109.

19   R. Izsák and F. Neese, *J. Chem. Phys.*, 2011, **135**, 144105.

20   S. Grimme, J. Antony, S. Ehrlich and H. Krieg, *J. Chem. Phys.*, 2010, **132**, 154104.

21   S. Grimme, S. Ehrlich and L. Goerigk, *J. Comput. Chem.*, 2011, **32**, 1456–1465.

22   S. Mai, F. Plasser, J. Dorn, M. Fumanal, C. Daniel and L. González, *Coord. Chem. Rev.*, 2018, **361**, 74–97.

23   F. Plasser, Theodore 2.0, http://theodore-qc.sourceforge.net.

24   F. Plasser, *J. Chem. Phys.*, 2020, **152**, 084108.

25   V. Tran, K. E. Allen, M. Garcia Chavez, C. Aaron, J. J. Dumais, J. T. York and E. C. Brown, *Polyhedron*, 2018, **147**, 131–141.